Industrial Backward Solution for Lead-Free Exempted AHP* Electronic Products
Part 1
User Context and Reliability Characterization

M. Brizoux, A. Grivon
Thales EPM
B. J. Smith, P. Snugovsky
Celestica Inc.

Abstract
Since the European 2002/95/EC RoHS directive enforcement on 1st July 2006, a dominating part of the electronic industry suppressed the use of Pb in electronic equipment. As one of the consequences, exempted industries like avionics, military and telecom servers are facing increasing SnPb component obsolescence issues. Before transitioning to the qualification and deployment of full lead-free for AHP electronic products, reliable backward solutions are urgently needed to overcome SnPb package procurement difficulties. The main concerns lie in Pb-free BGAs and SnBi leaded packages assembled with a conventional SnPb reflow soldering process which affects the solder joint microstructure and can compromise the 2nd-level reliability.

This paper deals with an extensive cooperation program between an EMS and an equipment maker engaged to evaluate the use of a specific "$SnPb^+$" assembly process as an option to solve the backward compatibility issues inherent to these kinds of components. The $SnPb^+$ process window as well as the incidence of reflow conditions on BGA mixed interconnects have been studied for a variety of generic components ranging from large plastic- and ceramic-BGAs down to 0.5mm pitch CSPs. The reliability has been assessed with statistics in comparison to full SnPb both under thermo-mechanical and mechanical stresses (vibrations, shocks) focusing on mission critical high-end applications in harsh environments. Numerous failure analyses have been conducted to evidence the failure modes and support the obtained reliability data.
This paper presents the –55°C/+125°C ATC reliability results of mixed BGAs assembled under various reflow conditions on dedicated test vehicles reflecting typical functional boards with the PCB finish as a variable (ENIG and Immersion Sn).
As a conclusion, results indicate that $SnPb^+$ is a very promising industrial solution for complex assemblies with long term mission in severe environments. Completion of the overall program including mechanical testing will permit to fully validate the use of the $SnPb^+$ process to secure the backward transition phase.

Note (*) AHP: Aerospace & High Performance

Introduction
Since July 1st 2006, the 2002/95/EC RoHS European directive has forced the electronic industry to switch from Tin-Lead to lead-free soldering alloys for components assembly.
Exemption domains have been defined for highly failure sensitive applications with long service lifetimes like military and aerospace because of the lack of knowledge on long term solder joint reliability in harsh environment. Furthermore, the physical properties of lead-free solder alloys (such as SAC) greatly differ from those of well known Tin-Lead so that well established accelerated tests can't be replicated for lead-free to forecast lifetime. These tests are not yet defined and moreover, the statistics of failure mechanisms and rates from the field are not sufficient to manage the reliability risk for many kinds of THALES products.
However, component manufacturers have changed their package finish to comply with the RoHS directive without taking into account AHP equipment makers due to their low share in volume. As a consequence we have to face this difficult situation: either manage the obsolescence by component storage with the great difficulty to forecast the customer demands, or find a solution to use lead free package finishes with standard Tin-Lead alloy, particularly sensitive with all kinds of BGA [1].
In the frame of our industrial policy, we have decided to share a cooperative and ambitious technological program with CELESTICA as a key partner in order to secure an industrial process solution called hereafter $SnPb^+$ (mixed metal assembly). This program is considered as key for both partners because we anticipate many years of mixed technologies before we can switch toward full lead-free assembly.

Backward solution overview
THALES has identified various generic solutions to address the lead-free BGA backward compatibility issue:

- Deballing/reballing (Package modification by replacement of BGA original SAC balls by SnPb spheres)
- Interposer (Package modification by addition of a carrier between the BGA and the board)

- $SnPb^+$ process (Assembly process modification, SnPb "like" global reflow process)

Despite serving the same objective, these generic solutions do have intrinsic different potentialities taking into account considerations like process window and complexity, cost, warranty, second-level interconnect reliability. To ensure having an acceptable reliable solution, we have evaluated the different options in parallel. $SnPb^+$ has been detected as the most promising in terms of industrialization, and as a consequence the most cost-effective.

Deballing/reballing has been fully qualified, with reliability performances as good as a standard Tin-Lead process. The main limitations are the cost, the limited number of subcontractors (often not integrated within an EMS) and the voiding of the IC manufacturer warranty as reballing involves extra post-delivery processes on the components [2].
The interposer solution intends to provide increased solder joint elasticity in thermo-mechanical fatigue through a higher stand-off obtained by mounting the original lead-free package onto an organic carrier with attached non-collapsible high-melt 90Pb10Sn spheres. The process, which is now well established and compliant with BGA pitches down to 0,5mm, is currently under investigation.

Backward program overview
In order to validate an industrially reliable $SnPb^+$ process, an extensive and comprehensive program has been built in close relationship with a worldwide EMS with the objective to measure the reliability of $SnPb^+$ mixed metal BGA assemblies in fatigue under both thermo-mechanical and mechanical stresses. This papers focuses on thermo-mechanical reliability results obtained in accelerated thermal cycling test (ATC).

For this part of the program, lead-free BGA packages with SnAgCu (SAC) balls have been assembled with two distinct processes:

- a standard SnPb reflow,
- a $SnPb^+$ reflow process specifically adjusted to ensure homogeneous mixing between the BGA ball SAC alloy and the SnPb solder paste while complying with maximum package temperature requirements of the IPC/JEDEC J-STD-020 specification. This demanding assembly process involves soldering temperatures higher than conventional SnPb but lower than a full SAC process. A full description of the process and its operating window is given in a separate companion paper (part 2 of this paper).

Numerous detailed post-assembly analyses have been carried out to evaluate the effect of the reflow profile on BGA joint mixing level and reliability. Possible effects of repair have been also included in the study with the addition of a dedicated repair process flow for one BGA type. As highlighted in the other paper, the main finding issued from the in-depth post-assembly characterization phase has been that the $SnPb^+$ profile ensured full mixing for all packages, whereas soldering temperatures of the standard SnPb profile lead to an insufficient mixing level and exhibited heterogeneous 2-part joints. Another outcome has been the increased voiding level in mixed solder joints compared to typical full SnPb for both PCB finishes and reflow profiles, which confirms observations from other publications [3]. Nevertheless, it has to be noted that this voiding level has been found to fully comply with IPC-A-610D requirements for all investigated parts.

To cover the widest spectrum of applications, the program integrated several variables for both components and printed circuit boards (PCBs).

First, a variety of generic BGA families have been included ranging from small 0.5mm pitch chip-scale-packages (CSP) up to higher thermal mass packages such as 42.5mm x 42.5mm Super-BGAs with heat spreader and large Ceramic-BGAs (CBGAs). Various ball diameters and SAC alloy compositions have been considered in the program, like SAC405 and SAC387.
Refer to table 1 for the full component description.

Second, two PCB surface finishes have been addressed: Electroless Nickel Immersion Gold (ENIG) and Immersion Sn. The purpose was to get reliability results with both kinds of intermetallic compounds involved in PCB soldering, namely $(Ni,Cu)_3Sn_4$ and Cu_6Sn_5. For the Immersion Sn finish, a minimum thickness of 1,2 µm has been specified to accommodate the hotter temperatures of the $SnPb^+$ reflow profile.

Table 1 – TV-ATC component list

Package Type	Number of Sites	Dimensions	Pitch	Finish
PBGA 1156	1	35mm x 35mm	1mm	SAC 405
CBGA 575	1	25mm x 25mm	1mm	SAC 387
CBGA 575	1	25mm x 25mm	1mm	90Pb10Sn
SBGA 560	2	42,5mm x 42,5mm	1,27mm	SAC 405
SBGA 560	2	42,5mm x 42,5mm	1,27mm	63Sn37Pb
µBGA 288	1	19mm x 19mm	0,8mm	SAC 405
CSP 132	1	8mm x 8mm	0,5mm	SAC 405
QFP 208	1	28mm x 28mm	0,5mm	97Sn3Bi
QFP 208	1	28mm x 28mm	0,5mm	SnPb
TSOP 54	1	22,22mm x 10,16mm	0,5mm	97Sn3Bi

TV-ATC test vehicle description

A dedicated TV-ATC test vehicle board has been designed and manufactured for the thermo-mechanical assessment.
The test vehicle boards have been designed to comply with the procured daisy-chain packages and the electrical monitoring system. BGA lands on the PCBs have been connected by pairs to match the corresponding package chained pattern and constitute a complete daisy-chain circuit. All solder joints of each individual BGA package have been chained together to a board-edge connector to enable continuous electrical monitoring. Grounding was of particular attention during the test vehicle design phase in order to avoid further noise disturbances and erroneous failure detection events during environmental testing.

On TV-ATC boards, routed channels around BGAs have been implemented to easily remove a single part immediately after failure detection during thermal cycling testing (see close-up view on figure 1). This configuration allows failure analyses in the early stage of crack initiation and development. Additional test pads have been added to facilitate failure isolation and identification by manual probing. These pads are typically placed based on our experience at critical places with highest probability of failures, such as BGA package and die outer edges.

A standard 1,6mm thick 12-layer PCB structure with 4 internal PWR/GND planes has been chosen to be representative of typical complex AHP applications. PCBs have been manufactured with a high-performance phenolic cured high-Tg FR-4 base materials with fillers compatible and qualified for lead-free soldering processes. This base material selection has been greatly oriented by the objective to evaluate interconnect reliability and avoid false failures caused by the PCB itself. An overview of the TV-ATC bare PCBs is given below (cf. figure 1).

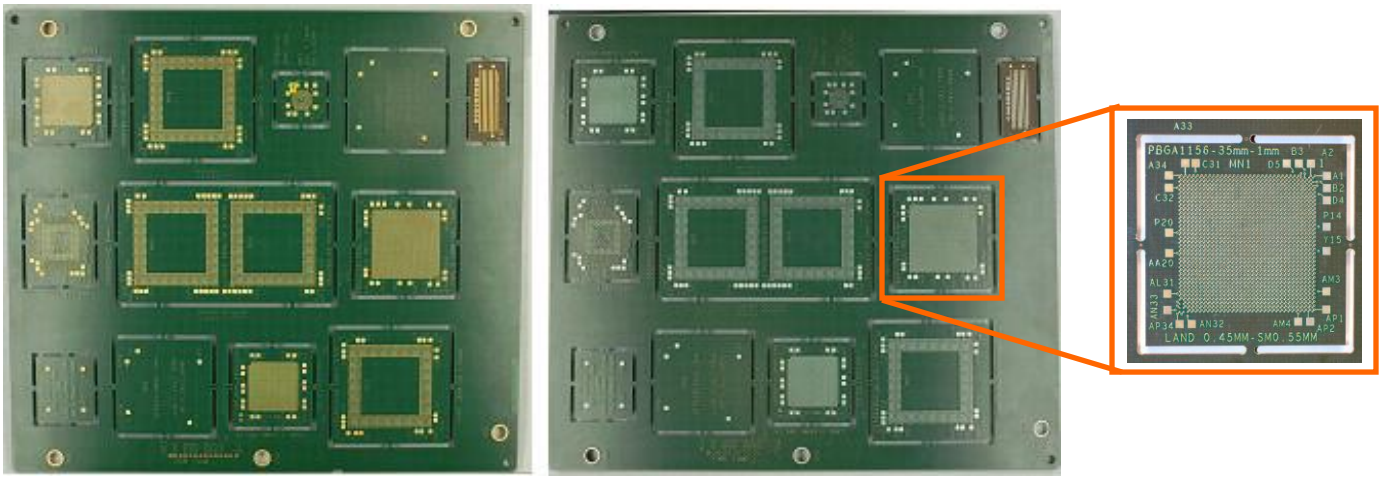

Figure 1 - TV-ATC topside overview with dual PCB finishes (left: ENIG; right: Imm. Sn)
Close-up view of the routed channels around components

Reliability test program and methodology

After the first phase of development and characterization of the $SnPb^{+}$ process, assemblies have been separately submitted to accelerated reliability tests under an air-to-air thermal cycling test. To produce consistent results and statistical failure

distributions, a population of 16 assemblies have been considered for each condition of the ATC testing (PCB finish, reflow profile).

The overall program has also been supported by a strict control of the manufacturing and testing conditions. As an example, the PCB manufacturing has been rigorously controlled by cross-sections before and after thermal stress to ensure the board quality and avoid further undesirable effects during environmental testing. Similarly, thorough efforts have been made for the ATC test set-up and realisation, especially in the field of :

- shielding and grounding of the electrical monitoring system to withstand noise interferences.
- temperature profile control to maintain constant upper and lower temperatures on the assemblies under test. Chamber settings have been permanently adjusted to compensate the variability of the oven thermal load due to failed component progressive extraction. This required the use of more than 80 thermocouples.

Thermal cycles were performed in a single-chamber oven under the most severe test conditions of the IPC-9701A specification, TC4, that is to say in the –55°C/+125°C range. Dwell times at lower and upper temperatures were set to 15 minutes for total cycle duration of 60 minutes (ramp-up and ramp-down rates of 12°C/min.). The testing duration was extended to more than 4000 ATC cycles in order to get a sufficient number of failures.

Figure 2 – ATC testing overview

Previous studies indicate that a proper continuous electrical monitoring system is critical to ensure an adequate failure indicator representative of field failures [4]. As a consequence, high-sampling rate event detectors were used to monitor the solder joint chains and the first transient event detected was considered the failure criterion. Multiple 256-channel test benches have been necessary for the overall test program.

Each intermittent event recorded by the detectors has been confirmed by a manual continuity check to ensure the presence of solder joint fracturing. This methodology enables avoidance of false conclusions and establishment of robust statistical failure distributions. In addition, destructive failure analyses with techniques such as dye & pry, cross-sections with optical and SEM observations have been conducted to determine the failure mechanisms for each package type.

ATC reliability test results and analysis

Reliability results have been established for each lead-free BGA package type by comparing the failure distributions of the two assembly process variants ($SnPb^+$ vs. standard SnPb) on Weibull plots. Plots have been normalized relative to the mean number of cycles to failure (N50%) of the standard SnPb assembly process distribution. Results have been also compared to existing internal data pertaining to the same package types in Tin-Lead version tested under similar conditions.

Mixed SAC 387 CBGA assemblies did not meet our reliability requirements and lead to much poorer fatigue results than usual CBGA assemblies with high-melt non-collapsible 90Pb10Sn spheres, whatever the reflow profile and mixing level in the component solder joints. An analysis of failed components has confirmed that failures correspond to typical solder joint crack near package interface (see figure 3 below). These expected poor performances are likely to account for a variety of factors, such as the lower stand-off height of the mixed solder joints which is known to be of primary importance for CBGA packages [2]. As a consequence, we consider that the $SnPb^+$ assembly process cannot be applicable for CBGAs and an alternate option has to be chosen to use CBGAs with SAC balls.

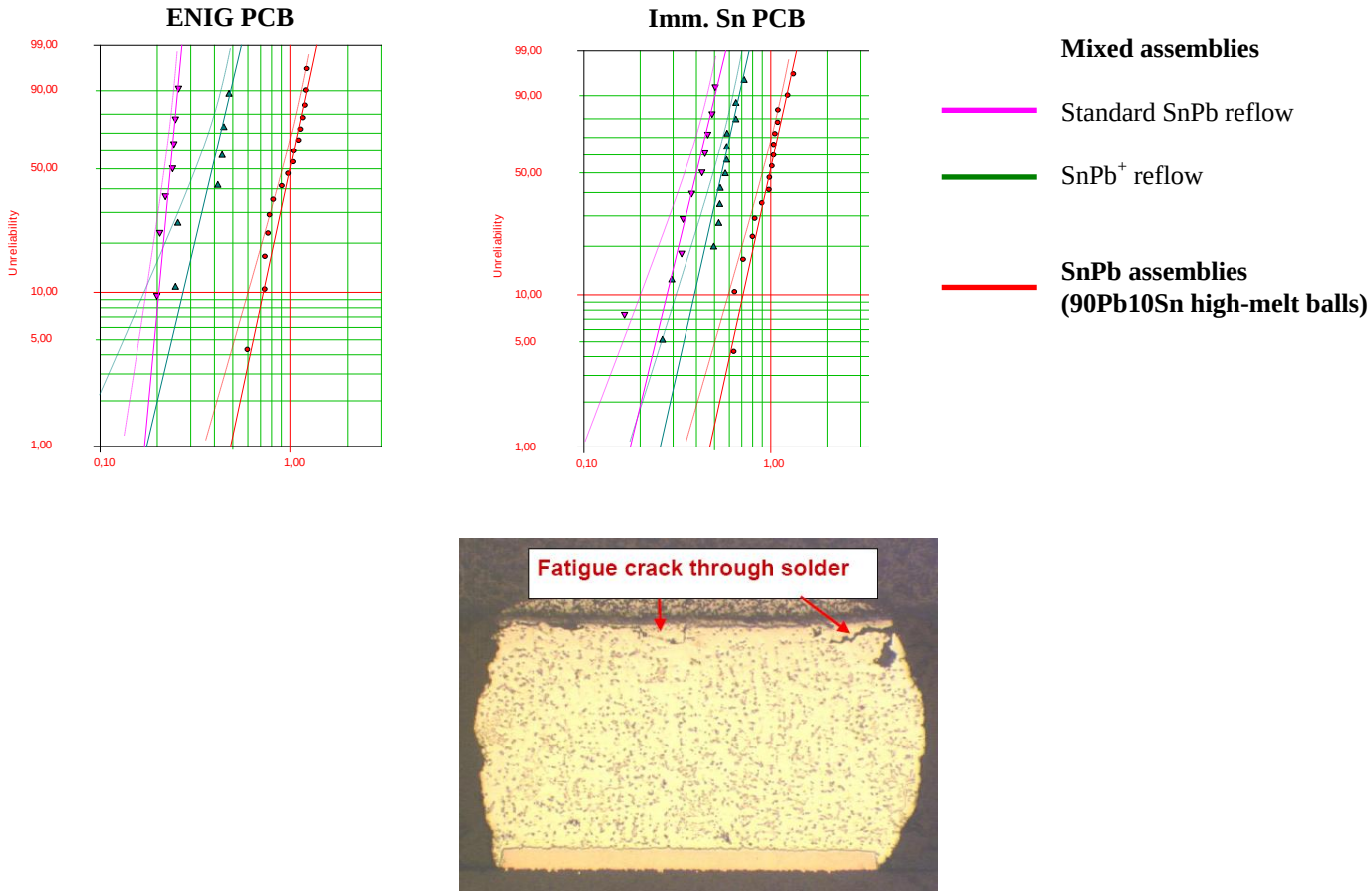

Figure 3 – Mixed CBGA ATC results & typical failure mode

For plastic BGA packages, a clear differentiation has been evidenced between the two reflow profiles:

- Standard SnPb assembly process gives unacceptable reliability results and generates premature failures
- $SnPb^{+}$ assembly gives satisfactory reliability results and even outperforms full SnPb

Early electrical failures have been noted on 2 different package types (large PBGA1156 and µBGA288) only with the usual Tin-Lead reflow profile. These failures occurred on about 3 out of 20 boards of each PCB finish either immediately after assembly or after a few dozens of cycles. Analyses revealed that the identified problems originate directly from a lack of joining between the SAC ball of the BGA and the Tin-Lead solder paste because of insufficient soldering temperatures. As illustrated on the pictures of figure 4, this phenomenon (often named 'head-in-pillow' effect) can have a random distribution, including in a same row of solder joints, and is hardly detectable in a production environment.

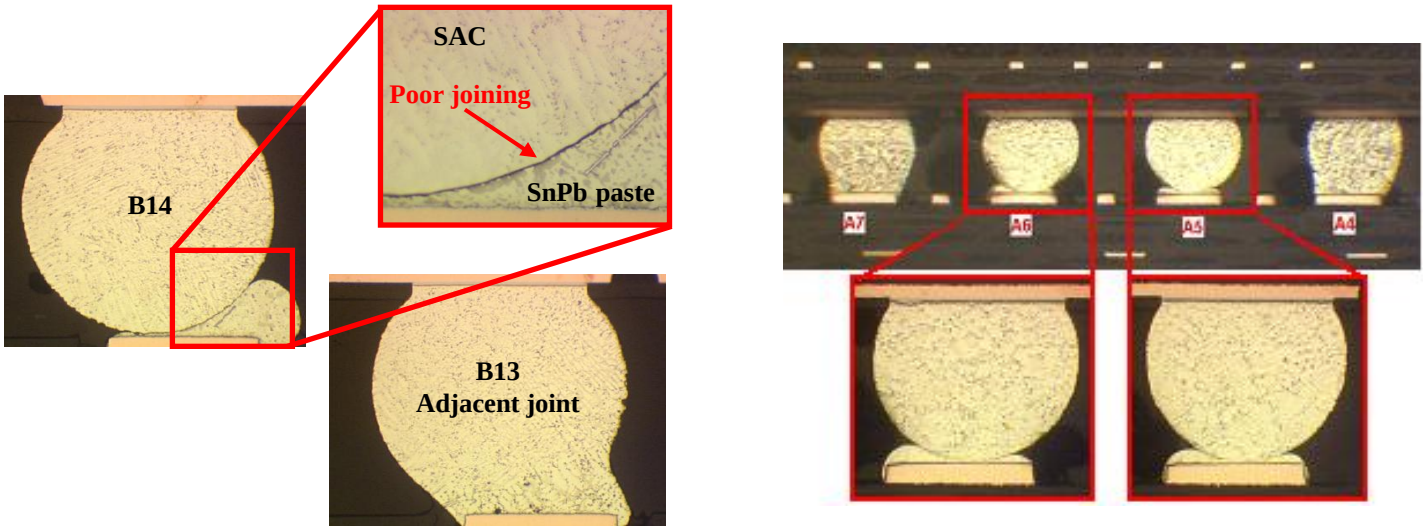

Figure 4 – PBGA1156 (left) & µBGA288 (right) failures due to insufficient reflow conditions. 'Head-in-pillow' phenomenon

For the 2 large PBGA packages of the TV-ATC board (PBGA1156 and SBGA560), the only few failures that have been recorded came in majority from boards assembled with the standard SnPb process (see table 2). The $SnPb^+$ repair process achieved on a SAC SBGA560 site has proven to have no influence on reliability, with only a few failures reported for both the repaired package itself and the adjacent SnPb SBGA.

Table 2 – ATC cycles to failure recordings for large PBGA1156 & SBGA560 mixed assemblies

Failures	ENIG PCB Finish				Imm. Sn PCB Finish			
	PBGA1156		SBGA560		PBGA1156		SBGA560	
	Std SnPb	$SnPb^+$	Std SnPb	$SnPb^+$	Std SnPb	$SnPb^+$	Std SnPb	$SnPb^+$
1		3011	1819	2070	601		2724	2803
2		4160	3808		1506			
3					1885			
4					2130			
5					2210			
6					3553			

The reliability results for the 2 smaller packages (µBGA288 and CSP132) are presented below (see figure 5).

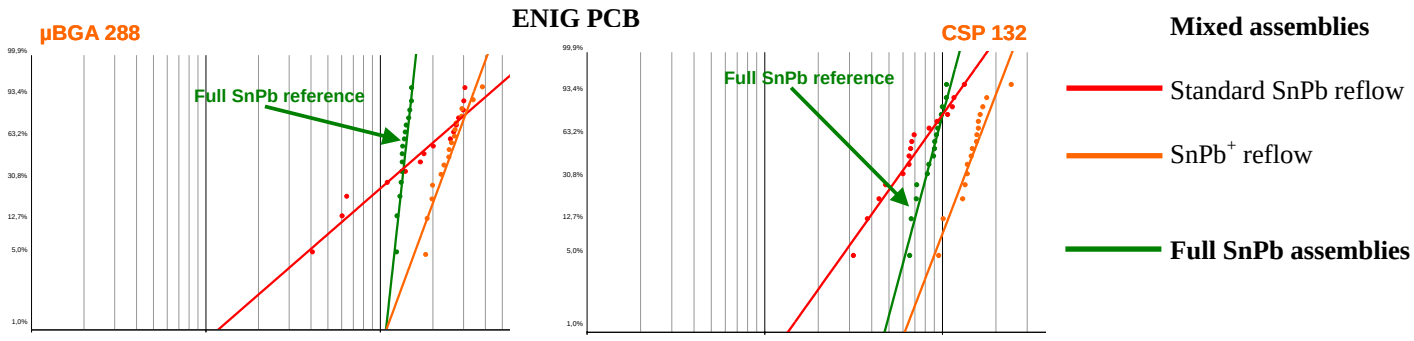

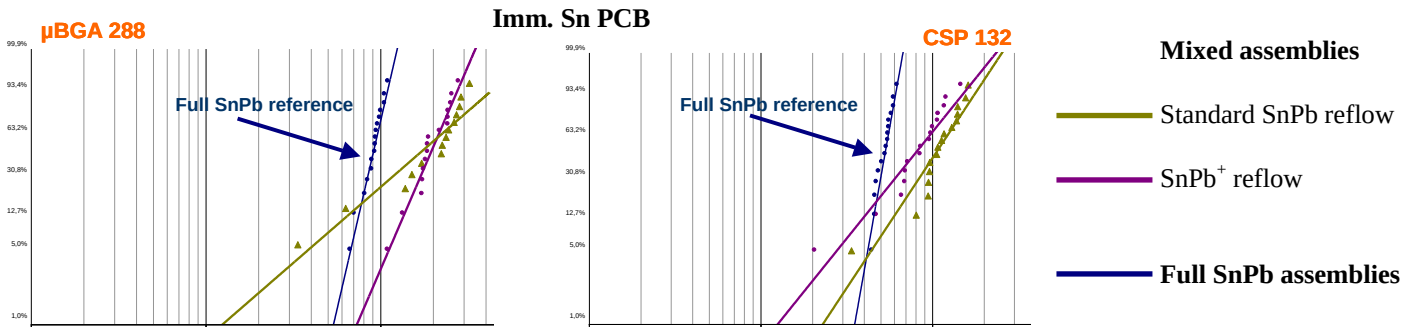

Figure 5 – Comparative Weibull plots for µBGA288 & CSP132 packages (top : ENIG PCB; bottom : Imm. Sn PCB)

For the ENIG PCB surface finish, the reliability obtained for BGAs assembled with the SnPb^{+} reflow profile clearly outperforms the full SnPb reference. Conversely, the same packages assembled with a colder standard reflow profile yielded poor results with a wider scatter (visible at the lower angle slope). To understand the better performances of mixed assemblies, one must remember that mixed assemblies involve lead-free BGAs with improved package constructions and materials (die-attach paste, molding compound) which induce a lower stress load on solder joints compared to full SnPb constructions. For instance, previous work has demonstrated that lead-free BGAs usually exhibit a much lower warpage than their SnPb equivalent counterparts under thermal excursions [5], thus potentially increasing solder joint fatigue resistance (see figure 6 below).

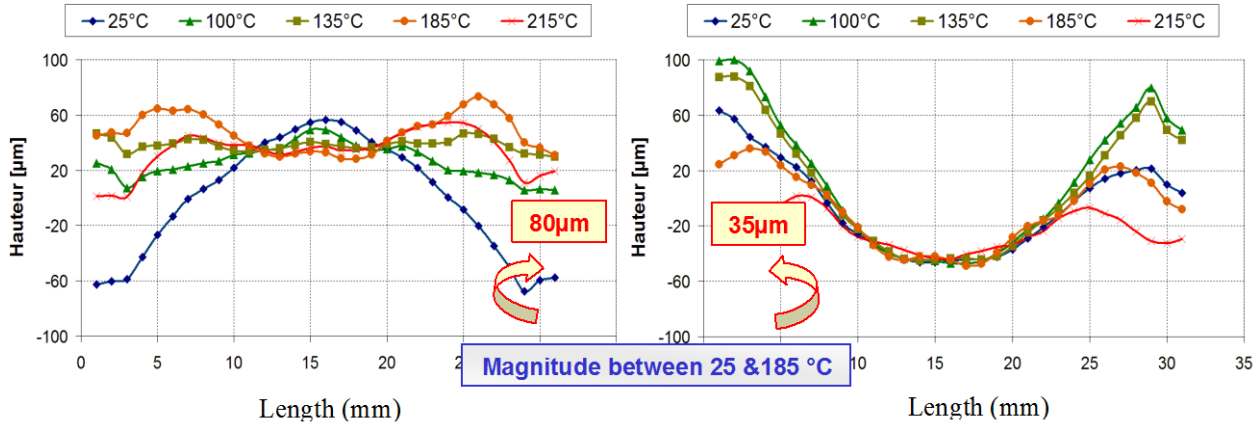

Figure 6 – Typical BGA package warpage at various temperatures (left : SnPb BGA ; right : equivalent lead-free BGA)
Note the SnPb BGA curvature changing with temperature (left) contrasting with the higher stability of SAC BGAs (right)

For the Imm. Sn PCB surface finish, the same conclusions can be drawn for the µBGA288 component with an identical relative ranking of the Weibull plots. However, a singularity has been noted for the CSP132 package: as shown in figure 5, the cumulative failure plots are very similar for the 2 reflow profiles and have a wider dispersion compared to the equivalent full SnPb baseline. Cracks or onsets of cracks have been identified near the lands of the CSPs assembled on Imm. Sn PCBs (see figure 6). Details of the failure analysis are given in the accompanying paper.

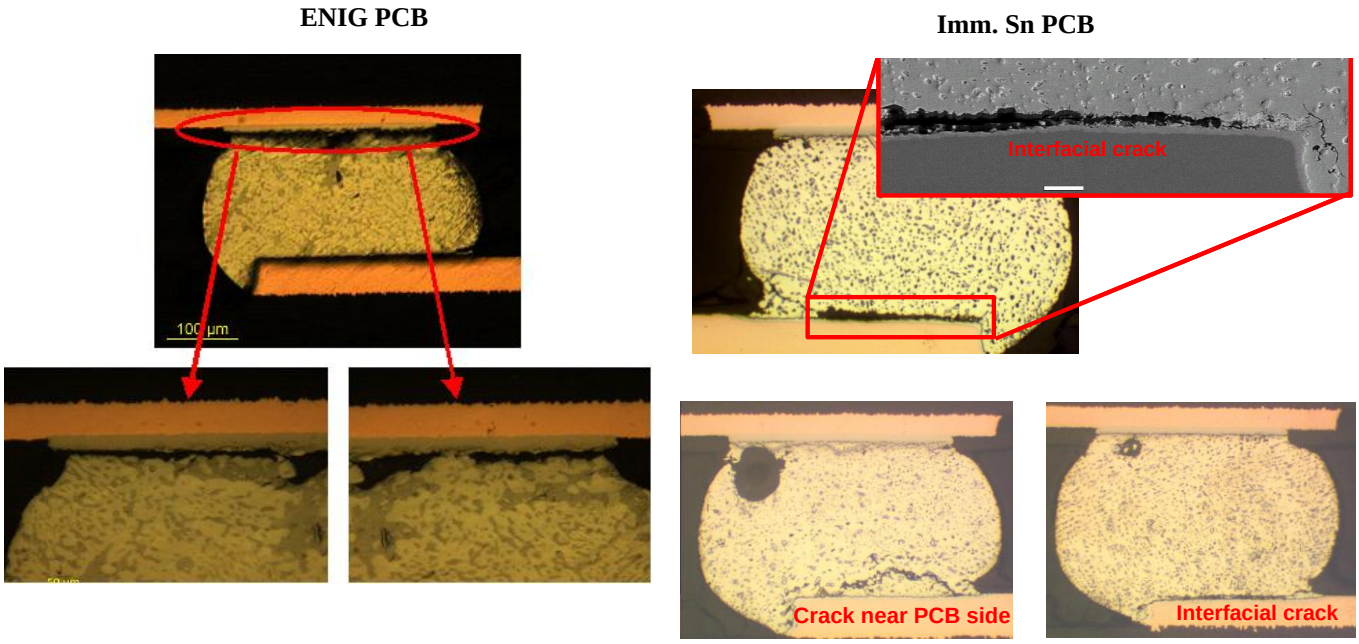

Figure 7 – Comparison of CSP132 failure modes :
typical fatigue cracking (ENIG, left) vs cracks near the PCB land (Imm. Sn, right)

Generally speaking, although backward mixed solder joints have been found to exhibit a voiding level slightly exceeding the conventional full SnPb baseline, analyses did not highlight any relation between the crack propagation and voids. In particular, only a marginal number of cracks extending through a void have been identified among the numerous analyses performed.

All the results obtained in the frame of this massive program indicate that a $SnPb^{+}$ reflow profile is mandatory to maintain the same reliability level as a full SnPb reference for all plastic BGA packages. As outlined, this process cannot be used for ceramic BGAs which require an alternative backward solution. We synthesized our conclusions in the table presented below.

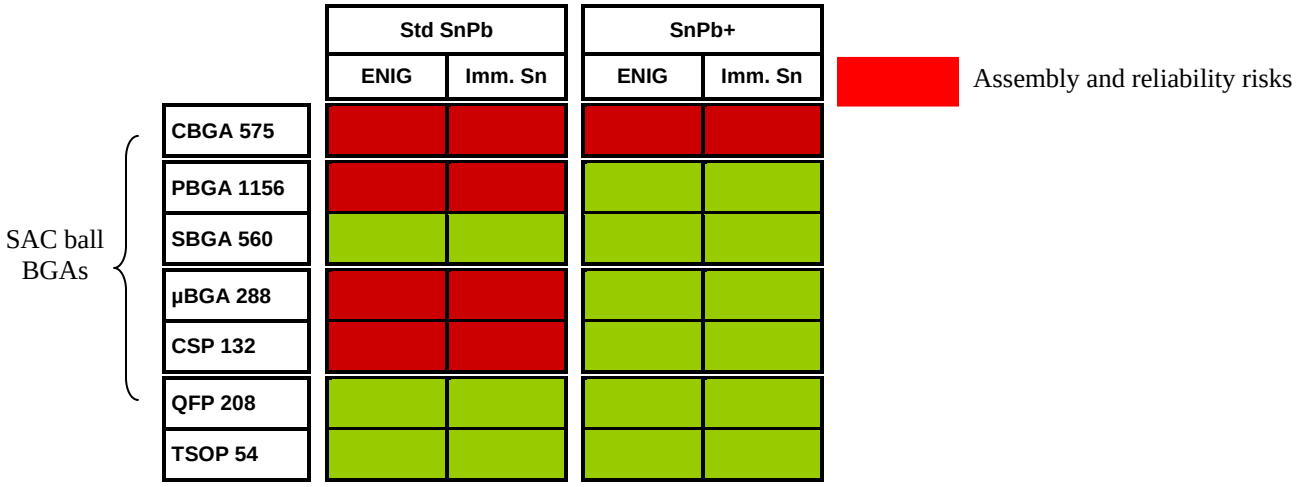

Figure 8 – Synthesis table of the $SnPb^{+}$ backward solution thermo-mechanical assessment

Conclusion

Since the banning of lead from electronic components and solder alloys in July 2006, AHP products have to face the obsolescence of Tin-Lead packages although they don't fall under the scope of the RoHS directive. The $SnPb^{+}$ backward solution mainly driven by area array packages becomes a mandatory technological brick which must be under control in order to secure the reliability risk for second level interconnects.

The long-term reliability results after very severe thermal cycle testing clearly show that the $SnPb^{+}$ process solution is much superior to the standard SnPb reflow profile. The solder joint reliability levels obtained have been found to be similar to the well known full SnPb process, with no significant impact of the PCB surface finish. The extensive backward reliability tests performed under industrial conditions and optimized reflow profile have given very good results. However, we must be aware that the $SnPb^{+}$ process window is much more reduced and critical than a standard full SnPb process, and that the voiding susceptibility is increased even if compliance with the IPC-A-610 class 3 requirements is maintained.

Reliability test under vibration and shock stresses are now on going before to release this backward solution for products subjected to severe mechanical conditions.

Acknowledgements
The authors would like to thank the following individuals from Thales EPM and Celestica: Julien Perraud and Florent Caperaa for post-assembly analyses, Jean-Guy Chesnay and Wilson Maia for their support in project management and technical guidance, Russell Brush for ATC testing and data analysis, Zohreh Bagheri for cross-sectioning and metallurgical analyses, Marianne Romansky, Thilo Sack, and Jeffrey Kennedy for fruitful technical discussions and manuscript revisions.

References

[1]. J.R. Wilcox, T.C. Godown, J.A. Adams, "Mixed Assembly: A Pb-Free Transition Strategy for Servers", IPC/Soldertec Global Conference on Lead Free Electronics, Barcelona, 2005.

[2]. W. C. Maia Filho, A. Grivon, M. Brizoux, "Evaluation of BGA Reballing Process as a Solution for Backward Issue", IPC/JEDEC Lead-Free Conference, Frankfurt, 2006.

[3] Jennifer Nguyen, David Geiger, Dr. Daniel Rooney, and Dr. Dongkai Shangguan, "Backward Compatibility Study of Lead Free Area Array Packages with Tin-Lead Soldering Process", IPC PC Expo, Los Angeles, 2006.

[4]. W. C. Maia Filho, M. Brizoux, H. Frémont, Y. Danto, "Improved Physical Understanding of Intermittent Failure in Continuous Monitoring Method", ESREF, Wuppertal, 2006.

[5]. M. Brizoux, H. Frémont, Y. Danto, W. C. Maia Filho, "Reliability Test Method Overview to Characterize Second Level Interconnects", IEEE EuroSimE, London, 2007.

Industrial Backward Solution for Lead Free Exempted AHP* electronic Products
Part 2
Process Technology Fundamentals and Failure Analysis

B. Smith, P. Snugovsky
Celestica Inc.
M. Brizoux, A. Grivon
Thales EPM

Abstract
This paper describes microstructures and thermal cycling performance of lead-free ball grid array and leaded components assembled with Sn-Pb solder using conventional SnPb reflow and reflow with temperature higher than 217°C to melt the lead-free ball and insure a full mixing (the $SnPb^{+}$ process). The work was part of a bigger project in conjunction with the paper "Industrial backward solution for Lead Free exempted AHP electronic products. Part 1. User context and Reliability Characterization", Michel Brizoux, Arnaud Grivon, Polina Snugovsky, Brian Smith published in the APEX2008 proceedings. The formation of uniform and non-uniform microstructures as a result of Sn-Ag-Cu (SAC) solder ball dissolution in a molten Sn-Pb solder using a conventional SnPb reflow or melting is studied. The difference in mechanisms and performance of uniform fully mixed and non-uniform partially mixed joints as a response on thermal cycling at -55°C to 125°C conditions is explored. Additional attention is paid to Sn-Bi finished QFPs and TSOPs. It is shown that Sn-Bi finish with 3 -5% Bi is not responsible for early failures if it is used with Sn-Pb solder.

Note (*) AHP: Aerospace & High Performance

Introduction
The introduction of recent environmental legislation prohibiting the use of hazardous substances in certain types of electronic products has had a major impact across the electronics industry supply chain. In response to this legislation, component suppliers have undertaken extensive re-engineering programs to ensure that their products comply with the new legislative requirements. Changes include the removal of lead from both lead frames and from solder balls in BGA applications. For electronic system producers manufacturing products that are either exempt or outside the scope of the legislation, and are not yet in a position to transition to lead free soldered product, the diminishing availability of older generation Pb containing devices presents a major concern. The issue is particularly acute with BGA packages. Faced with the withdrawal of Sn63Pb37 balled devices, producers have to engage in costly last time buys or post process components to replace the lead free balls with SnPb or attach the later versions of Pb free BGAs with Sn-Pb solder paste effectively giving a mixed alloy solder joint condition. Of these options, the mixed alloy approach is the most cost effective. Previous studies have demonstrated that by soldering joints at peak temperatures in excess of 217°C, Sn-Pb solder paste and Sn-Ag-Cu BGA balls completely mix to form a homogenous microstructure with adequate reliability performance (compared with full SnPb systems) for most electronic applications operating in benign field environment conditions [1-6]. However availability of test data simulating more extreme operating conditions such as aerospace applications is, at this time, very limited [7-11]. Furthermore, soldering BGAs at these elevated temperatures is likely to have a detrimental affect on other temperature sensitive components on older PCB designs.

This paper reports on the findings of a joint study between Celestica Inc and Thales EPM to evaluate the performance of mixed (SAC/SnPb) solder joints under harsh (-55°C to 125°C) accelerated temperature cycling conditions. The project assesses test vehicles built using two different reflow conditions and two surface finishes. A hotter profile is used to guarantee complete mixing of the solder joints by melting lead free solder balls above 217°C. A more standard SnPb profile with the temperature of the solder joints peaking below 217°C was also explored where most BGA joints exhibited only partial mixing between the SnPb solder paste and the Pb-free solder balls.

The study also included TSOP54 and QFP208 components with Sn-Bi and Sn-Pb finishes assembled with Sn-Pb solder using different reflow profiles. Previously published studies [12-15] on Sn-Pb-Bi system showed that the low melting reactions do not occur in the near eutectic Sn-Pb alloys with Bi additions up to 6% at the cooling rates employed at SMT processes. Therefore, there is no danger in using Sn-Bi finished components with Bi content up to 6%, that create final solder joints with Bi content 5 -10 times lower. Some concerns still exist in using Sn-Bi finishes in SMT processes that continue to still employ eutectic Sn-Pb solder. The concerns relate to the possibility of micro-segregation of Bi and non-equilibrium low melt structure formation in some conditions.

Experimental

Test vehicle

The accelerated thermal cycling (ATC) test vehicle is shown in Figure 1. The 12 layer board is 223mm x 233mm x 1.6 mm and was populated with 12 ball grid array /chip scale daisy chained packages. Component dimensions, I/O counts and solder ball composition are detailed in Table 1. Two batches of the test vehicle were produced, one with electroless nickel / immersion gold (ENIG) and the other with immersion tin (ImmSn). The test vehicle was designed to allow easy removal of failed components while maintaining capability to monitor electrical resistance on the daisy chains of the other devices.

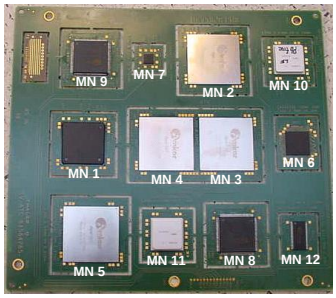

Figure 1. Test Vehicle.

Table1. Component Descriptions

Package	Ball or Finish	Dimensions, mm x mm	Pitch, mm	TV-ATC
CBGA 575	SAC 387	25 x 25	1.0	MN 10
	90Pb10Sn	25 x 25	1.0	MN 11
SBGA 560	SAC 405	42.5 x 42.5	1.27	MN 3
	63Sn37Pb	42.5 x 42.5	1.27	MN 2
PBGA 1156	SAC 405	35 x 35	1.0	MN 1
µBGA 288	SAC 405	19 x 19	0.8	MN 6
CSP 132	SAC 405	8 x 8	0.5	MN 7
QFP 208	97Sn3Bi	28 x 28	0.5	MN 9
	SnPb	28 x 28	0.5	MN 8
TSOP 54	97Sn3Bi	10.2 x 22.2	0.8	MN 12

Reflow profile set up

Two SMT reflow time/temperature profiles were used to assemble the boards. The profile settings selected were chosen to cover the temperature range that may be used in conventional SnPb manufacturing (SnPb profile) and an elevated temperature range that may be needed to accommodate lead free components in $SnPb^+$ assembly ($SnPb^+$ profile). The maximum temperature of the SnPb profile was targeted to not exceed 216°C to ensure that the lead-free balls would not melt. The second ($SnPb^+$) profile was designed to ensure that all components experienced a minimum solder joint peak temperature of 220°C. Thermo couples were attached to the top side of each component, to an outer corner joint and, for the larger BGAs, to a central joint in order to accurately monitor temperatures. Profiling and subsequent assembly of the boards was carried out using a 3.8m long, 10 heating zone conveyorised reflow oven. Temperature profiles for each component are detailed in Table 2.

The SnPb profile temperatures ranged from 206 °C in the inner joints of the PBGA1156 to 215°C in the µBGA 288 and CSP132. The peak reflow temperatures for the $SnPb^+$ profile were in the 221 – 239°C range for the solder joints. The times above the Sn-Pb liquidus (TAL) of 183 °C were not longer than 107 seconds. The temperatures on the top side of the components in the $SnPb^+$ assembly vary from 222°C to 239°C. Thus the $SnPb^+$ profile complies with maximum package temperature requirements of the IPC/JEDEC J-STD-020 standard. Although this profile is hotter than a standard SnPb, its temperature range is lower than for pure lead free SAC assembly with the minimum solder joint temperature 232°C.

Table2. Reflow profile characterization.

			SnPb Profile			$SnPb^+$ Profile		
Ref	Component Description	Thermocouple Position	Rise Time 120-160°C (mm:ss)	Time Above 183°C (mm:ss)	Peak Temp (°C)	Rise Time 120-160°C (mm:ss)	Time Above 183°C, (mm:ss)	Peak Temp (°C)
MN1	PBGA1156 SAC	Central Ball	1.18	1.22	206	1.17	1.35	221
		Outer Ball	1.36	1.36	213	1.36	1.42	234
		Body	1.19	1.18	207	1.20	1.26	225
MN3	SBGA560 SnPb	Central Ball	1.24	1.25	209	1.23	1.36	230
		Outer Ball	1.27	1.29	210	1.26	1.38	231
		Body	1.29	1.28	210	1.28	1.33	231
MN4	SBGA560 SnPb	Central Ball	1.24	1.25	209	1.23	1.36	230
		Outer Ball	1.29	1.31	210	1.28	1.38	231
		Body	1.25	1.24	209	1.25	1.34	230
MN6	uBGA288 SAC	Central Ball	1.14	1.42	215	1.13	1.46	237
		Outer Ball	1.14	1.44	215	1.15	1.45	237
		Body	1.14	1.45	218	1.11	1.41	239
MN7	CSP132 SAC	Central Ball	1.16	1.41	215	1.17	1.47	239
		Body	1.15	1.40	215	1.15	1.45	239
MN8	QFP208 SnBi	Lead	1.31	1.31	211	1.31	1.35	231
		Body	1.17	1.20	207	1.16	1.30	226
MN10	CBGA575 SAC	Central Ball	1.22	1.23	207	1.22	1.32	225
		Outer Ball	1.26	1.23	209	1.25	1.30	227
		Body	1.20	1.18	206	1.15	1.23	223
MN11	CBGA575 SnPb	Central Ball	1.20	1.24	206	1.20	1.34	226
		Outer Ball	1.26	1.24	207	1.25	1.31	228
		Body	1.13	1.16	203	1.13	1.23	222
MN12	TSOP54 SnBi	Lead	1.14	1.42	216	1.14	1.45	236
		Body	1.13	1.41	216	1.15	1.44	236

Standard Sn63Pb37 no clean solder paste deposited using a 0.125mm thick nickel electroformed stencil was used to assemble the boards. All boards and components were baked for 24 hours at 125°C in accordance with J-STD-033.

Prior to building the complete set of test vehicles, 4 boards in an advanced batch were assembled and subsequently analyzed to assess the degree of mixing between solder paste and ball alloys. The main batch was split into 4 cells of 20 boards each - SnPb profile/immersion tin finish, SnPb profile/electroless nickel-immersion gold, $SnPb^+$ profile/immersion tin, $SnPb^+$ profile/electroless nickel-immersion gold.

Accelerated Temperature Cycling

16 boards from each profile/surface finish cell were exposed to accelerated thermal cycling. The cycling profile applied was -55°C to + 125°C with a 60 minute cycle (27 minute hot dwell, 23 minute cold dwell, 5 minute ramps). All devices were continuously monitored for resistance through their daisy chain using event detectors. Failing devices were cut out of the boards within 160 hours of a failure being detected and the boards replaced back in the ovens for further cycling. Failure analysis was conducted on selected components including the first two failures per component type, for each of the ENIG and ImmSn cells. The last failures were also cross-sectioned and analyzed to confirm the failure mode. The failing solder joints were cross-sectioned. After 4000 cycles, some failed and some surviving BGA joints were subjected to dye-and-pry test analysis.

Failure Analysis

As-assembled and thermal cycled solder joints were examined using optical microscopy, X-ray (Phoenix PCB analyzer), scanning electron microscopy (SEM, Hitachi S-4500 and SEM Hitachi S-3000N), and X-ray spectroscopy (Oxford EDX). Differential Scanning Calorimetry (TA DSC 2910) analyses were performed to study ball grid array solder joint melting after partial or complete mixing of the Sn-Pb solder with lead-free balls during assembly. The DSC was also used for leaded component melting characterization.

Results and Discussion

Microstructure Formation

Ball Grid Array

X-Ray examination

X ray analysis was used to quantify the extent of voiding within the mounted BGA/CSP devices. In general, voiding was within acceptable levels (Table 3) and was greater in devices with SAC balls compared to those produced with SnPb balls. A slightly greater level of voiding was seen in the components soldered with the hotter reflow profile. No clear pattern emerged in comparing voiding levels on the two different PCB surface finishes.

Table 3. Voiding characterization.

Component Type	Surface Finish	Profile	Voids, %					
			20	19-17	16-12	11-8	7-4	3-0
CSP132	ENIG	SnPb^{+}	+ (20.1%)	+	+	+	+	+
CSP132	ENIG	SnPb			+	+	+	+
CSP132	ImmSn	SnPb		+	+	+	+	+
µBGA288	ENIG	SnPb^{+}			+	+	+	+
µBGA288	ENIG	SnPb				+	+	+
µBGA288	ImmSn	SnPb					+	+

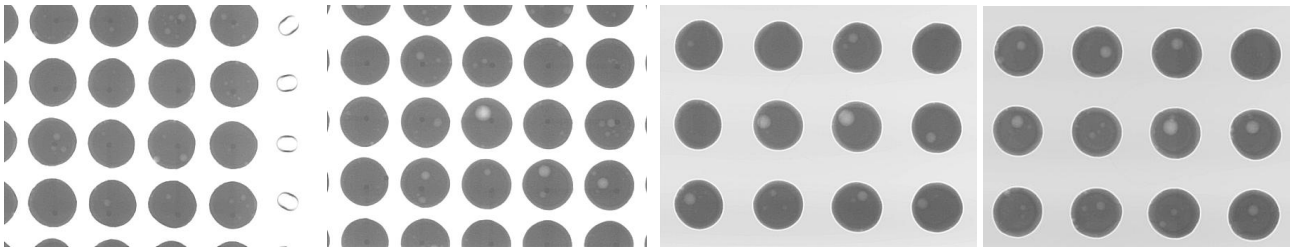

a **b** **c** **d**

Figure 2. Comparison of voiding on SAC balled components, ImmSn: a - CBGA 575,SnPb profile; b - CBGA 575, SnPb^{+} profile; c – µBGA 288, SnPb profile; b - µBGA 288, SnPb^{+} profile.

In order to compare the degree of mixing and the microstructure of solder joints assembled using the Cold and SnPb^{+} profiles, samples were optically examined and then cross-sectioned.

Theory of mixing

It is expected that during reflow when Sn-Pb solder melts at 183°C, the Sn-Ag-Cu, solder ball will begin to dissolve in the molten solder (Fig. 3a, b). The theory of mixing is described in [2]. The dissolution continues until the liquid attains a saturation composition. The saturation level increases with rising temperature. The higher the temperature, the larger the portion of the SAC solder ball that is consumed by the molten Sn-Pb solder. For a certain ratio of SAC solder ball and Sn-Pb solder, full mixing or dissolution is possible below the melting temperature of 217°C for Sn-Ag-Cu solders (Fig. 3 d, e), assuming the time above liquidus is sufficient. The mixed Sn-Pb-Ag-Cu liquid solder solidifies during cooling stage of the reflow. Partially or fully mixed solder joints can form (Fig. 3 c, d) depending on the reflow profile, Sn-Pb / SAC ratio, and solder joint size.

If the reflow peak temperature reaches 217°C the Sn-Ag-Cu solder ball starts melting and full mixing can be achieved for all components independent of solder joint size or Sn-Pb paste / SAC ball ratio (Fig 3 g – i).

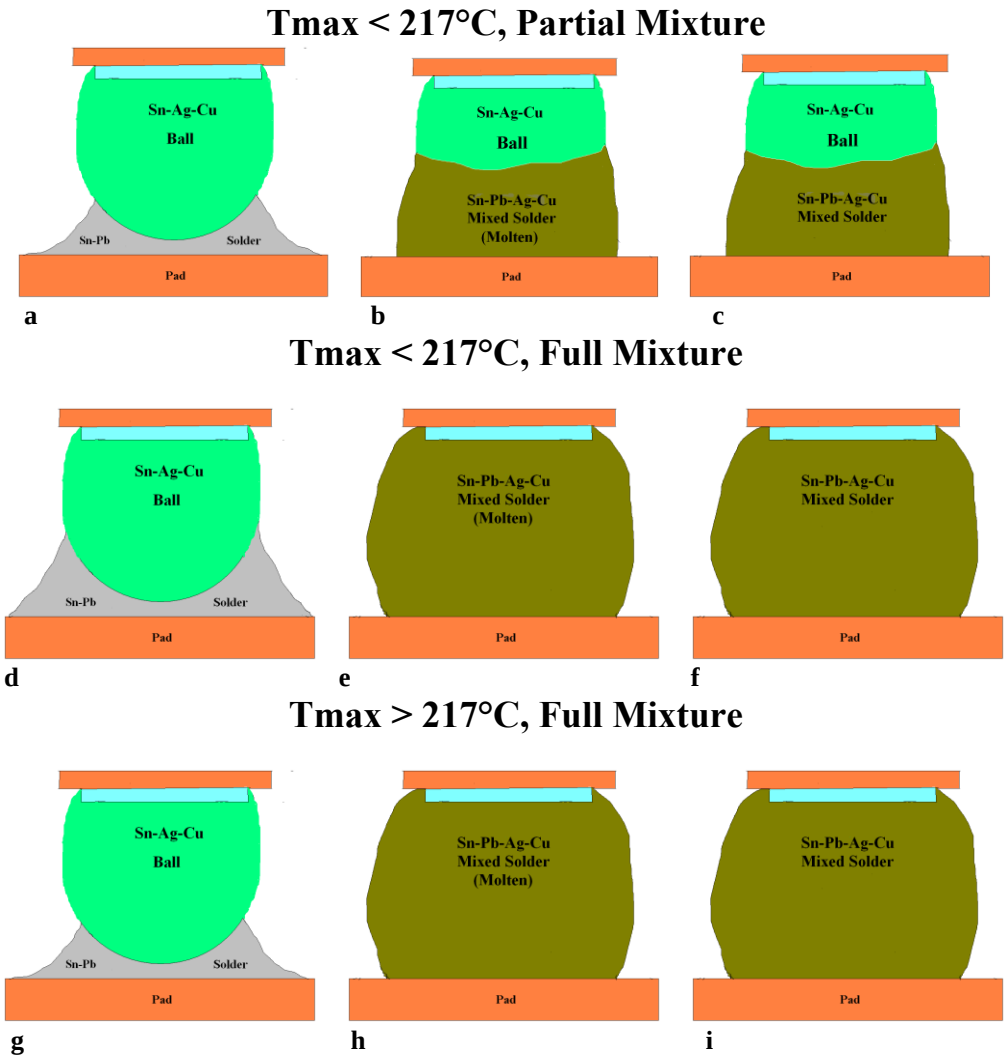

Figure 3. Schematic of Sn-Pb solder / SAC ball reflow metallurgy showing three possible scenarios - with Tmax (maximum reflow temperature) below 217°C, partial mixture (a – c); Tmax below 217°C, full mixture (d – f); Tmax above 217°C, full mixture (g – i): a, d, g - before reflow; b, e, h - during reflow; c, f, i – after reflow.

SnPb profile

The examination of components assembled using the colder reflow profile revealed that for the CBGA 575, SBGA 560 and large plastic PBGA 1156, the solder joints did not exhibit complete mixing. These joints reflect the reflow conditions shown in Figure 3 a - c and had two distinct microstructures: the part of the SAC ball that was not dissolved and the portion that was fully mixed (Figure 4). The undissolved SAC ball structure is similar to the typical SAC ally structure and contains primary-like Sn dendrites and $Sn+Ag_3Sn+Cu_6Sn_5$ ternary eutectic in the interdendritic spaces. The mixed solder, on the other hand, has Sn dendrites that are much larger in size, binary Sn+Pb, and ternary $Sn+Ag_3Sn+Pb$ or quaternary $Sn+Ag_3Sn+Pb+Cu_6Sn_5$ eutectics between the dendritic arms. A Sn rich band is clearly visible between these two areas of the solder joint.

A similar microstructure was observed in the SBGA 560 and PBGA 1156 components (Fig. 5a), although each exhibited different degrees of mixing: 30 – 50% for the PBGA 1156 and 35 – 45% for the CBGA575 and SBGA 560. The corner joints were exposed to higher temperatures during assembly (Table 2) so therefore had better mixing than joints in the centre of the components.

Smaller components assembled using the SnPb profile, experienced higher temperature than the larger CBGA, SBGAs and PBGAs. The 215°C (132 TAL) that the CSP reached during SnPb reflow was enough for full mixing (Fig. 5 b), as depicted in Figure 3 d – f. The CSP's SAC solder balls were completely consumed by the molten Sn-Pb. The resulting liquid solder crystallized forming uniform microstructure with evenly distributed Sn, Pb, Ag_3Sn, and Cu_6Sn_5 phases across the joint.

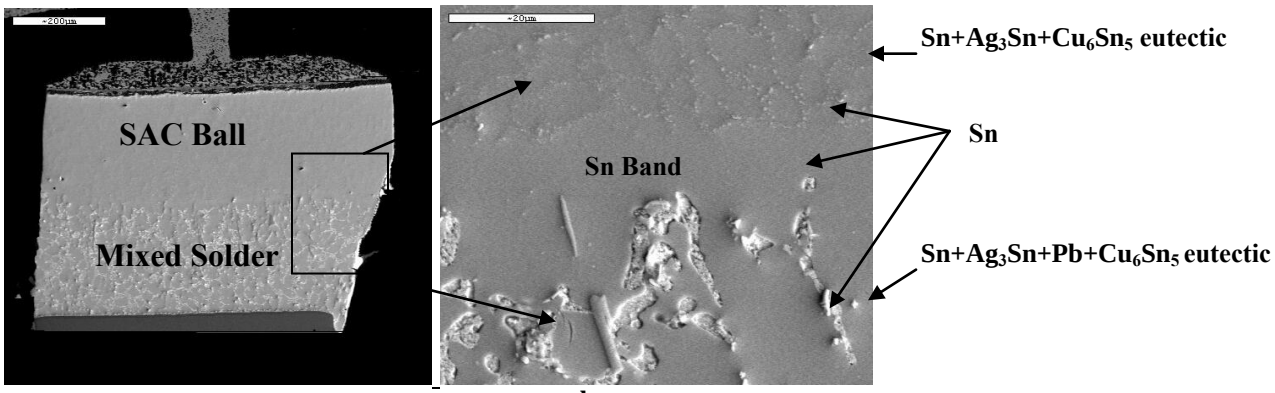

a b

Figure 4. Microstructure of CBGA 575 solder joints produced with peak temp 209°C, SEM: a - 100x; b – 2000x.

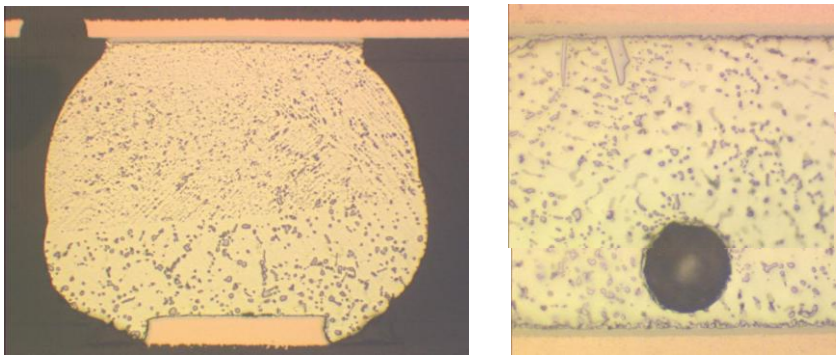

a **b**

Figure 5. Microstructures of partially and fully mixed solder joints produced using SnPb profile: a – PBGA 1156, 100x; b - CSP 132, 400x.

The same reflow parameters only produced partial mixing for the μBGA 288. The corner and most of the outer layer joints were fully mixed. At the same time some other joints, especially in the centre of the component, were not fully mixed (Fig. 6). The degree of mixing varied from 70 to 100%. Even if the remains of the SAC ball are not visible, the microstructure of the solder joint is not uniform across the joint. The component side of the joint contains more Sn phase whereas the board side has more eutectics (Fig. 6 a). The Sn dendrite arms are distinctively larger at the component side of the joint.

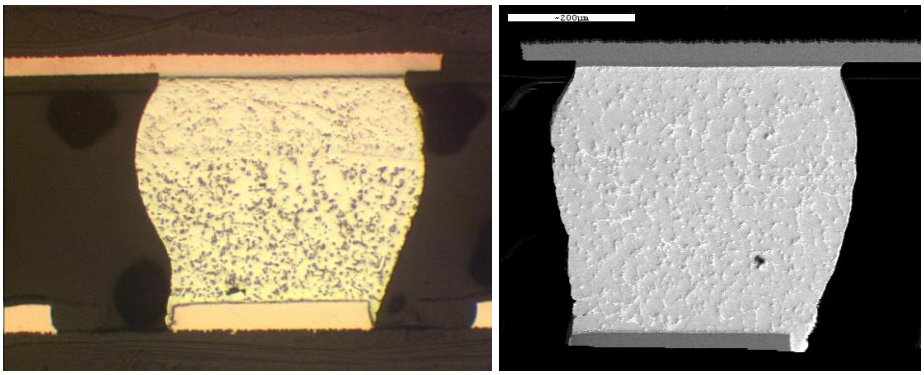

a **b**

Figure 6. Microstructures of μBGA 288 produced using Cold profile: a - 100x; b - SEM, 130x.

The origin of this non-uniformity is the same as for the Sn band in partially mixed joints (Fig.4 b, 5 a, 6 a) and discussed in more detail in [16]. The resulting Sn-Pb-Ag-Cu composition has a very large pasty range (Fig. 7). It varies depending on Sn-Pb solder paste / SAC ball ratio. The μBGA 288 pasty range was the widest among the components analyzed in the study. The melting of μBGA 288 solder joints formed using the SnPb profile starts at 176.7°C and stops at 220.3°C (Fig. 7 a) . In the fully mixed joints formed in the $SnPb^{+}$ profile assembly, the melting range is 34°C (Fig. 7 b). The CSP 132 joints have the narrowest solid – liquid zone - 28°C (Fig. 7 c). The PBGA 1156 zone width is in the 30°C range (Fig. 7 d).

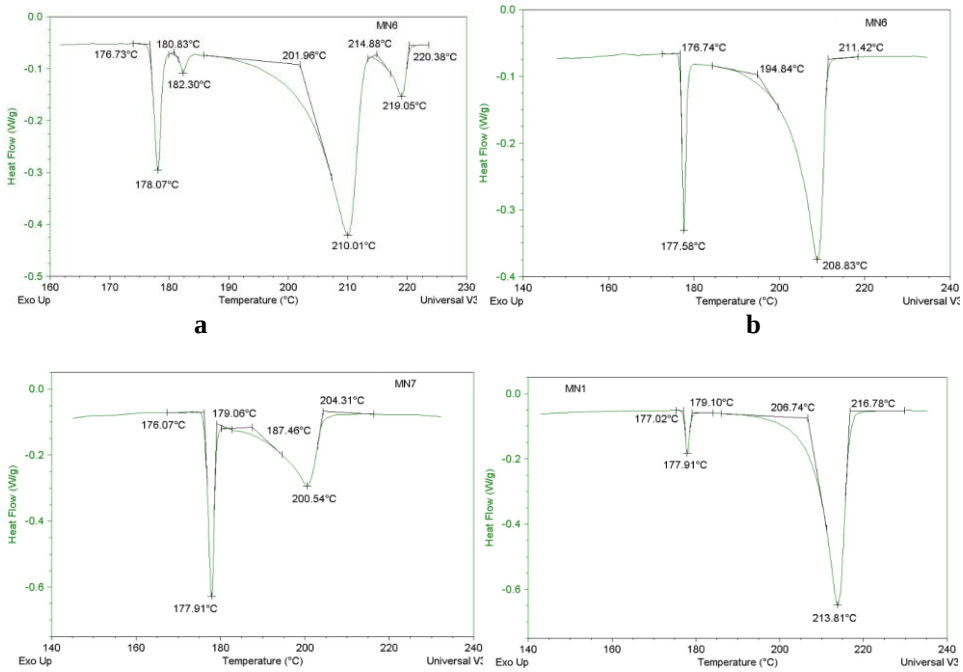

Figure 7 DSC heating curves: a - µBGA 288, SnPb profile; b - µBGA 288, SnPb$^+$ profile; c - CSP 132; d - PBGA 1165.

Phased solidification occurs across this entire temperature range starting with Sn dendrite formation, followed by Sn+Pb and/or more complex Sn+Pb+Ag_3Sn ternary or even Sn+Pb+Ag_3Sn+Cu_6Sn_5 quaternary eutectics. The Sn phase originates from the existing Sn in the remaining SAC ball or from the clusters in the higher Sn content liquid immediately after its dissolution facilitating the Sn nucleation. The solidification proceeds towards the board side forming a zonal microstructure. The last portion of liquid, that contains more eutectic, solidifies at the board side and looks like a Pb-rich zone.

There was no observed difference in the degree of mixing in solder joints formed on ENIG and ImmSn.

SnPb$^+$ profile

Complete mixing was achieved in all ball grid array components mounted on the boards using the SnPb$^+$ reflow profile. The balls were melted and mixed with Sn-Pb molten solder (Fig. 3 g-i) forming uniform microstructures (Fig. 8). The structure also contains, as was shown for the SnPb profile, primary Sn-dendrites and eutectic. The binary Sn+Pb, ternary Sn+Pb+Ag_3Sn and /or quaternary Sn+Pb+Ag_3Sn+Cu_6Sn_5 eutectics occupy the interdendritic spaces. The SnPb$^+$ reflow microstructure is finer. The sizes of the Sn dendritic arms, Pb patches and Ag_3Sn and Cu_6Sn_5 intermetallic particles are smaller. Figure 9 illustrates this comparison between CBGA 575s assembled with peak temperature 227°C (SnPb$^+$ profile) and 209°C (SnPb profile). The Sn dendrite arms at least 3.5 times larger in Cold profile joints.

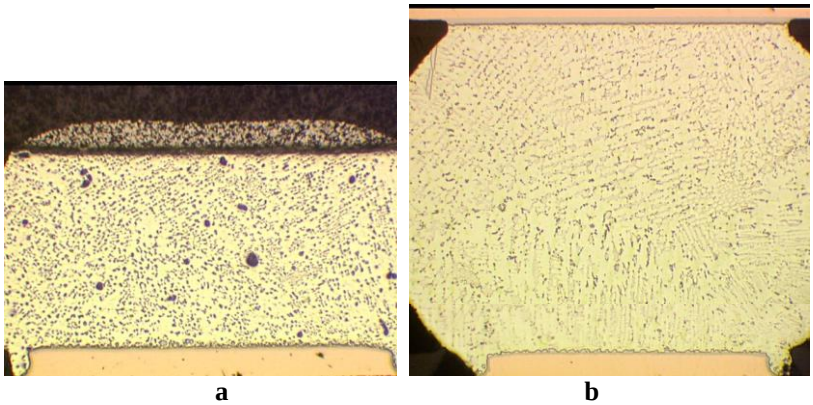

Figure 8. Microstructures of fully mixed solder joints produced using SnPb$^+$ profile, 100x: a –CBGA 575, SEM; b – SBGA 560.

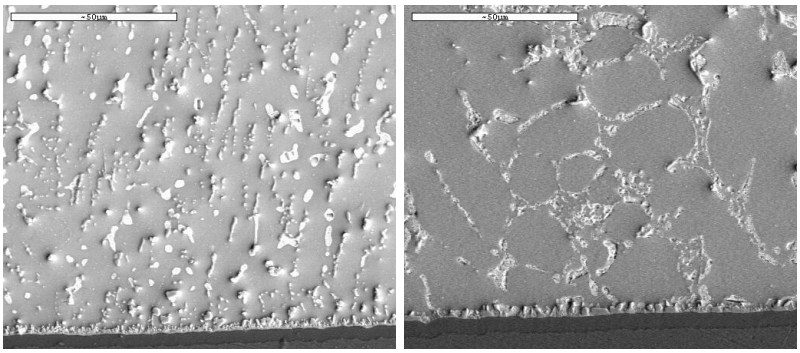

a b

Figure 9. Comparison of CBGA 575 microstructures produced using $SnPb^+$ profile (a) and SnPb profile (b), SEM, 1000x

Leaded Components

The microstructure of QFP 208 with Sn-Pb and Sn-Bi finishes is shown in Fig. 10. Sn-Pb finished components have a eutectic microstructure (Fig 10 a) with some primary-like Pb crystals. In Sn-Pb solder joints with Sn-Bi component finish, Sn-primary crystals are clearly visible (Fig. 10 b). A similar microstructure was described previously [12, 13]. It reflects a higher Sn content in the resulting solder after a dissolution of the 90%Sn – 3%Bi component metallization layer. The thicker the surface finish layer, the more Sn dissolves into the solder, driving it further from the eutectic composition. Cu dissolving from the ImmSn finished PWB in both QFP 208 and TSOP 54 cases resulted in the presence of Cu_6Sn_5 particles (Fig. 11). The number of these particles is slightly higher in the components after $SnPb^+$ reflow. No Cu_6Sn_5 particles were found in solder joints formed on ENIG boards.

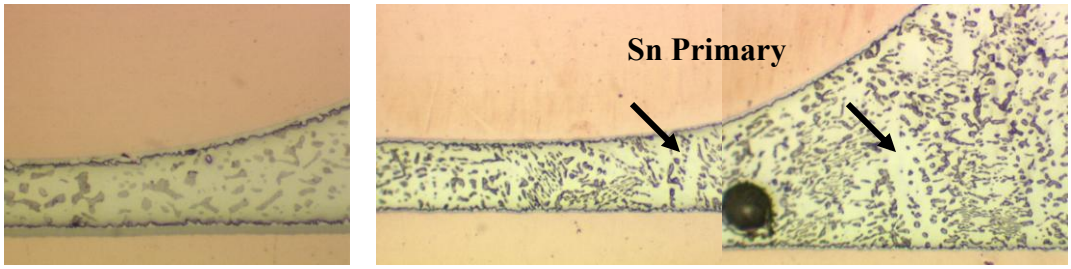

a b

Figure 10. Comparison of QFP 208 solder joint microstructure with different finishes, 400x: a – Sn-Pb finish; b –Sn-Bi

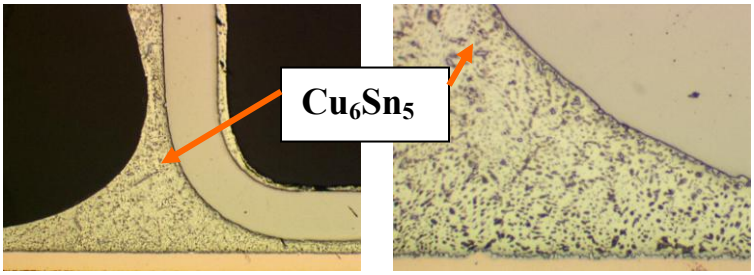

a b

Figure 11. TSOP 54 microstructure containing Cu_6Sn_5 particles: a – 100x; b – 400x

The QFP 208 and TSOP 54 solder joints with Sn-Bi finished leads were carefully examined using SEM, EDX and DSC. No evidence of the low melting structure containing Bi-Pb compound particles was found. The DSC analysis of solder joints with Sn-Bi finished leads formed on ImmSn boards revealed only the $Sn+Pb+Cu_6Sn_5$ eutectic that melts at about 177°C and binary Sn-Pb eutectic (181 – 184°C) (Fig. 12 a, c). The DSC curves for leaded components with Sn-Pb finish were similar to those for Sn-Bi (Fig. 12 b). There is also a primary Sn phase (184 - 190°C) in the Sn-Bi QFP joints shown in Fig 10, and a primary Pb phase (184 - 188°C) in Sn-Pb finished QFPs. The difference in microstructure formed on ENIG boards that does not contain Cu_6Sn_5 was clearly reflected in the DSC curves. These curves do not have troughs at about 177°C indicative of the $Sn+Pb+Cu_6Sn_5$ eutectic (Fig 12 d).

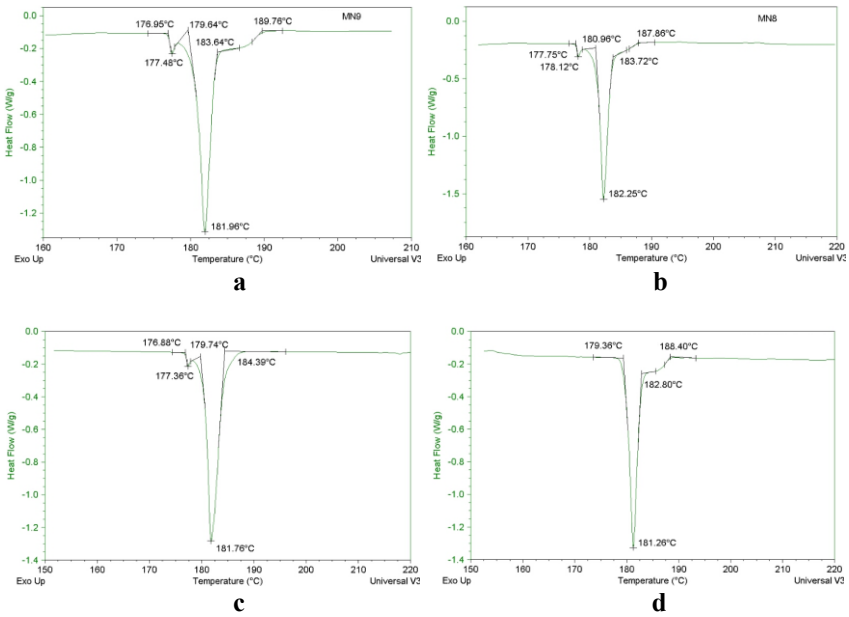

Figure 12. DSC heating curves for leaded components, Cold profile: a QFP 208 with Sn-Bi lead finish, ImmSn; b – QFP 208 with Sn-Pb lead finish, ImmSn; c – TSOP 54 with Sn-Bi lead finish, ImmSn; c – TSOP 54 with Sn-Bi lead finish, ENIG.

Thermal Cycling Results and Failure Analysis

For the purposes of presenting the ATC reliability results, the components were grouped as shown in Figure 13. The reliability data for CBGA 575 can be found in the accompanying paper Part1. For those components with sufficient failures after 4000 cycles, the resulting failure data was statistically analyzed using two parameter Weibull models. Specific Weibull parameters which will be compared include shape or slope (β – beta), and the characteristic life (η - eta), which is the number of cycles required to cause failure of 63.2 % of the samples from a particular cell. From these values, the numbers of cycles for a 1% failure rate is extrapolated. This is very important for high reliability products.

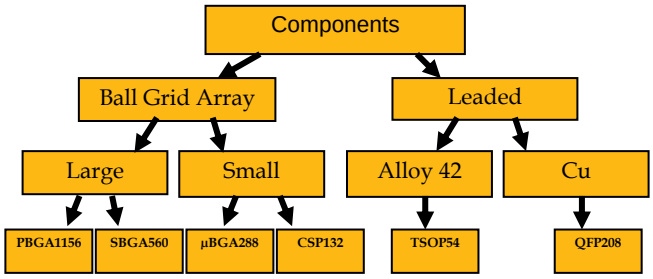

Figure 13. Component grouping for ATC reliability discussion.

Ball Grid Array

Large components

The ATC results for the PBGA 1156 are shown in Table 4. The components assembled using the $SnPb^{+}$ profile with full mixing of the SAC405 ball and Sn-Pb solder paste only started failing after 3000 cycles at -55°C to + 125°C on ENIG finished boards and exhibited no failures even after 4000 cycles on ImmSn finish. Partially mixed joints formed using the SnPb SMT profile mounted to ENIG boards had also not failed after 4000 cycles. On the contrary, partially mixed joints assembled on ImmSn boards failed early. The Weibull plot for the SAC PBGA 1156 assembled with Sn-Pb solder paste using a conventional Sn-Pb reflow (Cold profile) has a characteristically low β slope (Fig. 14), the cause of which is explained below.

Many interfacial crack failures were observed (Fig. 15 a). The detailed SEM analysis showed that cracks propagated through the Pb-rich layer (Fig. 15 b, c). The formation of this layer is described in the "Microstructure Formation" section, "SnPb profile" paragraph. During reflow cooling, solidification begins at the interface of the remnants of the undissolved SAC solder ball, with Sn dendrites growing towards the hot board side. The liquid, which is gradually enriching with Pb and Ag and depleting of Sn, finally crystallizes as binary and then ternary eutectic in interdendritic spaces. The last portion of liquid

solidifies as a ternary eutectic at the board side when the temperature of that region reaches about 177°C. Any additional constituents resulting from dissolution of substrate material, such as organic and inorganic additives that were co-deposited with Immersion Sn, will segregate in the last portion of liquid. Therefore, the interface between the intermetallic layer and bulk solder may be insufficiently strong to withstand stresses experienced during thermomechanical testing.

Table 4. ATC results for SAC405/Sn-Pb PBGA 1156.

Number of Failures	Cycles to failure			
	SnPb, ENIG	$SnPb^+$, ENIG	SnPb, ImmSn	$SnPb^+$, ImmSn
1		3011	601	
2		4160	1506	
3			1885	
4			2130	
5			2210	
6			3553	

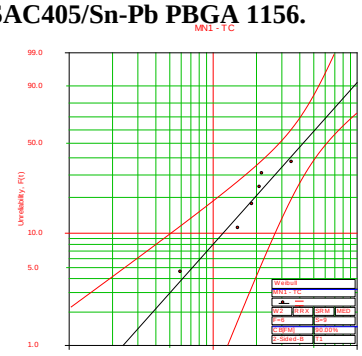

Figure 14. Weibull plots for mixed SAC405/Sn-Pb PBGA1156, SnPb profile, ImmSn.

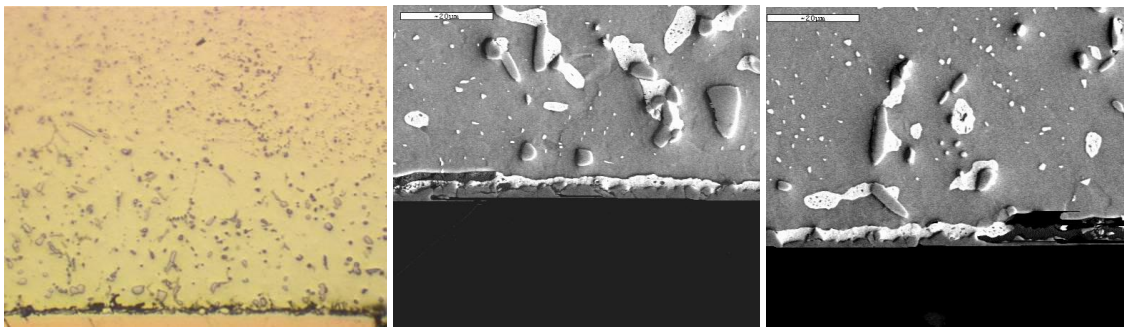

a **b** **c**

Figure 15. Microstructure of PBGA 1156 assembled using SnPb profile after thermal cycling, -55°C to 125°C cycling: a - 605 cycles, 200x; b – 2165 cycles, SEM, 1500 x; c- 2165 cycles, SEM, 2500x.

Two lead-free (MN4 and MN5) and two Sn-Pb (MN2 and MN3) SBGA 560 components were assembled on each board. The MN4 joints were reworked to compare to the non-reworked MN5. The influence of rework on adjacent MN3 was also analyzed. The ATC results for the SBGA 560 are shown in Table 5 and Figure 16. Very few failures occurred in SAC405 SBGA 560 components (Table 5) whereas all 16 pure Sn-Pb devices for three combinations and 15 for one combination of reflow profiles and surface finishes failed (Figure 16 a, b). The incubation period – the time before failure was similar for mixed SAC/Sn-Pb and pure Sn-Pb joints, but the rate of failure was much faster for the pure Sn-Pb system. It indicates a significant difference in β slope between the mixed and pure Sn-Pb assemblies. With lower β slope in SAC/Sn-Pb joints early failure are statistically expected.

There was no significant influence of rework on adjacent Sn-Pb component detected (Fig. 16 a, b). The failure mode for both adjacent and non-adjacent joints is typical fatigue fracture at the component side (Fig. 17a). Secondary cracks were also found on the board side. Mild nickel corrosion was visible on some of the pads (Fig. 17 b).

From both pure Sn-Pb graphs on Figure 16 a and 16 b the difference between ImmSn and ENIG finish is clearly visible. ImmSn outperforms ENIG by a factor of about 1.5. There is no difference between conventional Sn-Pb reflow (SnPb profile) and reflow at the higher temperature ($SnPb^+$ profile) for the components mounted to the Immersion Sn finished boards. There is a marginal improvement in reliability using the higher reflow temperatures for ENIG boards. This may be explained by proper wetting on the ENIG corroded areas.

More reworked mixed SBGA 560 components failed than non-reworked, but the number of failed components (maximum 5 out of 16) was much smaller than for pure Sn-Pb. The Weibull analysis indicates a low β (Fig. 16 c). The detailed failure analysis is in progress. It is believed that this behavior is as a result of a non-uniform microstructure that may be formed during solidification when a temperature gradient between the component and board sides exists.

Table 5. ATC results for SAC405/Sn-Pb SBGA 560 (MN5).

Number of Failures	Cycles to failure			
	SnPb, ENIG	$SnPb^{+}$, ENIG	SnPb, ImmSn	$SnPb^{+}$, ImmSn
1	1819	2070	2724	2803
2	3808			

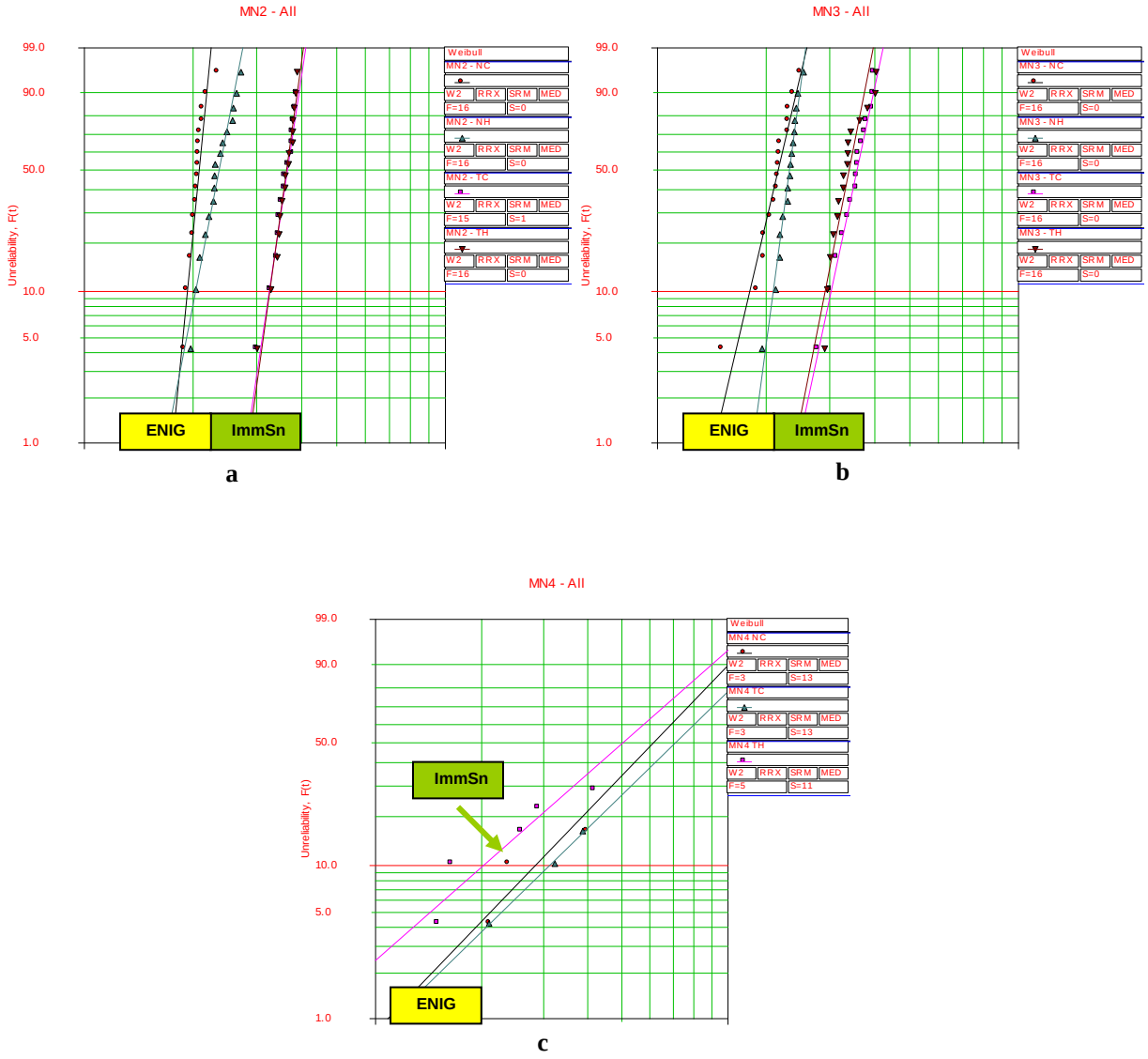

Figure 16. Weibull plots for mixed SBGA 560: a – pure Sn –Pb; b – pure Sn-Pb adjacent to the reworked mixed SBGA 560; c – mixed SBGA 560 reworked.

Summarizing the ATC results for large components for extended reliability applications it would be possible to conclude that for completely mixed SAC ball/Sn-Pb solder joints, the $SnPb^{+}$ profile has comparable fatigue life to that of Sn-Pb and that for partially mixed joints, the SnPb profile may also have acceptable reliability unless some microstructure anomalies such as ternary eutectic with high Pb-content and defect accumulation between the intermetallic layer and the bulk solder occur.

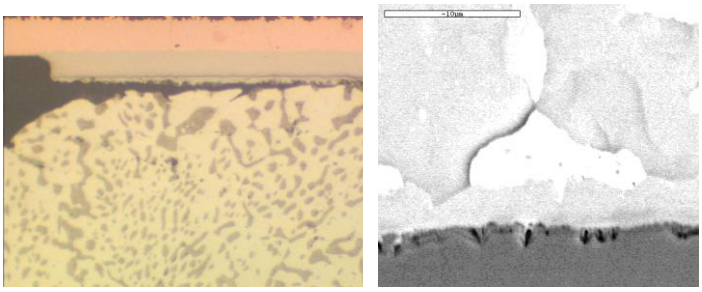

a b

Figure 17. Typical failure mode of pure Sn-Pb SBGA 560 (a) and evidence of mild corrosion on the nickel layer (b): a - 400x; b – SEM, 5000

Small components

The ATC results for small components are shown in Figure 18. They were also compared to the internal Thales data for the same package type in SnPb version tested under similar conditions. The difference in behavior between the fully and partially mixed joints is clearly visible for the µBGA 288 (Figure 18 a, c). ImmSn and ENIG Weibull plots for the SnPb$^+$ profile are parallel and have greater β than for conventional Sn-Pb reflow (SnPb profile) by a factor of 3.4 and 1.8, respectively. The failure mode of the first fails is crack propagation between the intermetallic layer and the bulk solder (Fig. 19 a) through the area solidified from the last portion of liquid as was described for large BGAs. Secondary cracks grow through the remainder of the balls at the components side (Fig. 19 b). The latter failures for the SnPb profile and all failures for the SnPb$^+$ reflow occur through the recrystallized solder on the component side (Fig. 19 c). The fully mixed solder joints in the SnPb$^+$ assemblies outperform pure Sn-Pb joints. Contrary to the SnPb$^+$ assemblies, partially mixed joints formed using the conventional SnPb profile have much poorer reliability than reference pure SnPb.

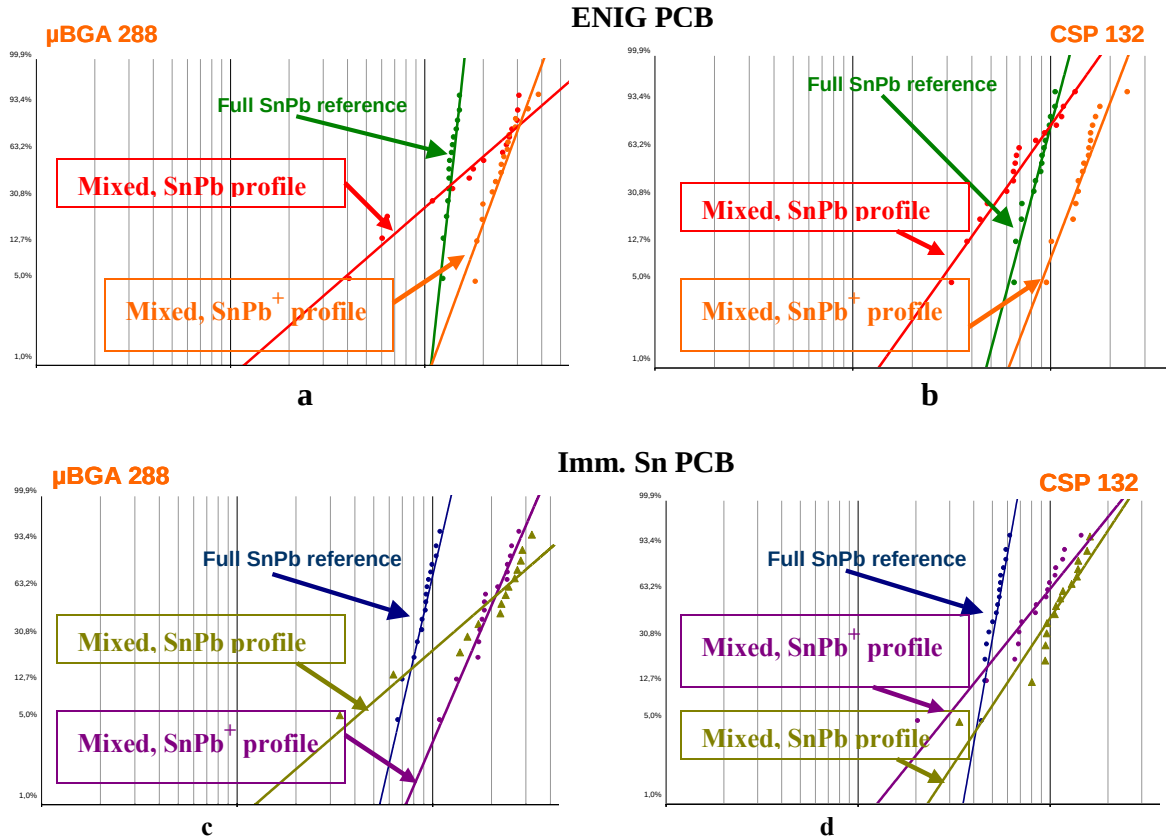

Figure 18. Weibull plots for µBGA 288 (a, c) and CSP 132 (b, d).

In the CSP 132 cells where SAC balls were fully mixed with Sn-Pb solder, there was no statistically significant difference between cycles to failure of solder joints formed on ImmSn using the SnPb$^+$ and SnPb profiles. In terms of early failure these components behave slightly worse than pure SnPb. There is however, a significant difference in the ENIG cells. The performance of the CSP 132 assembled using the SnPb$^+$ reflow is much better. It also outperforms pure SnPb components.

The failure mode for the CSP 132 is predominantly fatigue cracking at the component side (Fig. 20 a). Secondary interfacial cracks are also present. In some cases, the failure occurs due to interfacial fracture (Fig. 20 b) at the PWB side. This type of failure was mostly detected for the conventional SnPb profiles in ImmSn and ENIG cells, but was also found in early failed joints formed on ImmSn using $SnPb^+$ reflow. This interfacial failure looks similar to failures described earlier and also propagates through the layer enriched with Pb. More work should be done to better understand the mechanism of this type of failure.

The best reliability for both the µBGA 288 and CSP 132 was achieved on ENIG finished boards using the $SnPb^+$ reflow profile. Usually solder joints which form an intermetallic with Cu due to the PWB surface finish (ie.OSP, Immersion Ag, HASL etc.) are stronger than joints formed on Ni surfaces (i.e. ENIG etc). Pure Sn-Pb joints in this project (Fig. 16 a, b), assembled on same boards, have much higher reliability with ImmSn. This suggests that the combination of mixed composition and surface finish plays an important role in microstructure formation.

In summary for small components, it is important to stress that complete mixing and uniform microstructure are necessary requirements for acceptable reliability. These characteristics are achievable using $SnPb^+$ profile.

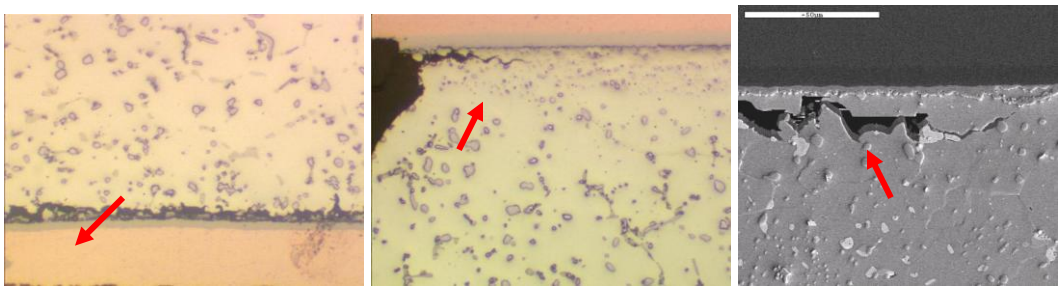

a **b** **c**

Figure 19. Microstructure of µBGA 288 after thermal cycling, -55°C to 125°C cycling: a – SnPb profile, ENIG, 420 cycles, 400x; b – SnPb profile, ImmSn, 342 cycles, 400x; c - $SnPb^+$ profile ENIG, 2098cycles, SEM, 1000x.

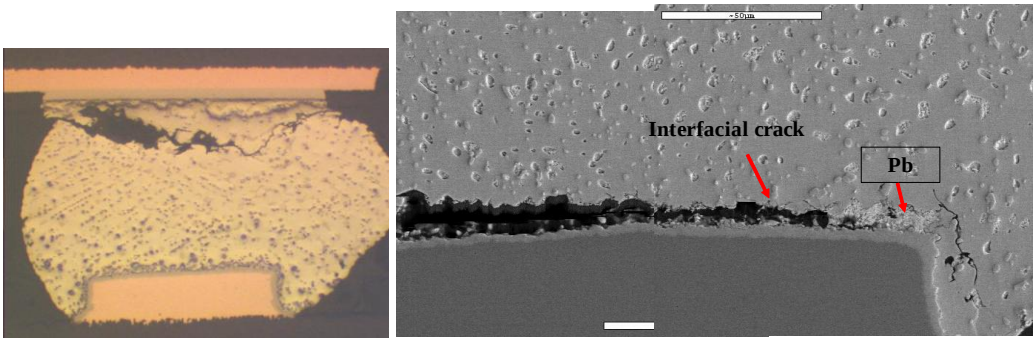

a **b**

Figure 20. Microstructure of CSP 132 after thermal cycling, -55°C to 125°C cycling: a – $SnPb^+$ profile, ENIG, 984 cycles, 100x; b – SnPb profile, ImmSn, 987 cycles, SEM, 1000x.

Leaded Components

QFP 208

There were very few failures of this component in thermal cycling. As a result, it is not possible to assess whether different reflow profiles or surface finishes influences reliability. The performance of each of the eight cells is excellent. The thermal cycling results (Table 6) are in agreement with industry published report [15].

Table 6. ATC results for QFP 208

QFP finish	Cycles to failure			
	SnPb, ENIG	$SnPb^+$, ENIG	SnPb, ImmSn	$SnPb^+$, ImmSn
Sn-Pb		2360	2042	2250
Sn-Bi	2408	3081		3249

TSOP 54

The thermal cycle results for the TSOP 54 are shown in Figure 21. As expected, the reliability of TSOP components with the alloy 42 lead frame material is reduced compared to QFP with the copper lead material because of the great CTE mismatch [15].

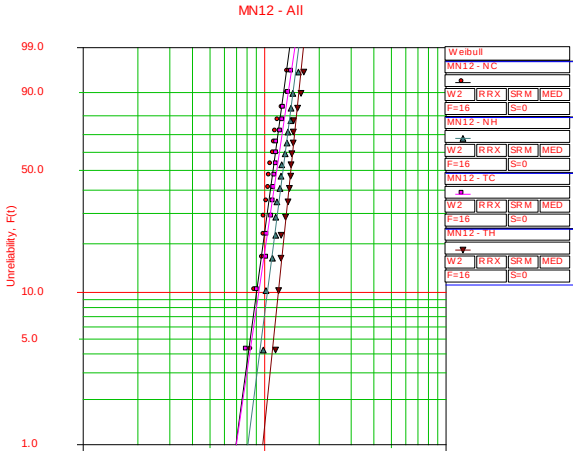

Figure 21. Weibull plots for mixed TSOP

There were no anomalies detected in thermal cycling of the components assembled on both ENIG and ImmSn finishes using the SnPb and SnPb$^+$ profiles. The statistical analysis showed that all the data points belong to the same population for each cell. The data from this study (Table 7) are similar to the thermal cycle results published by Dave Hillman on TSOP with Sn-Bi and Sn-Pb finish assembled using Sn-Pb solder [15].

Table 7. ATC results for TSOP

TSOP finish	Cycles to failure									
	SnPb, ENIG		SnPb$^+$, ENIG		SnPb, ImmSn		SnPb$^+$, ImmSn		Data from [15]	
	First Failure	Mean Life	First Failure	Mean Life	First Failure	Mean Life	First Failure	Mean Life	First Failure	Mean Life
Sn-Pb									1125	1381
Sn-Bi	850	1158	982	1313	802	1220	1148	1448	945	1172

Hot reflow slightly outperforms conventional assembly for both ENIG and ImmSn finishes (Fig. 21). This is thought to be a result of a more homogenous distribution of the high Sn (97%Sn) component finish material. The best thermal cycling reliability was demonstrated for the solder joints assembled on Immersion Sn finished boards using the SnPb$^+$ reflow profile. Both Mean Life and First Failure are better than reported [15] for TSOPs with Sn-Pb lead finish (Table 7).

The observed failure mode is typical for a TSOP with Alloy 42 lead frame material. The crack propagates through a coarsened band starting from the heel fillet and growing through the solder along the grain boundaries close to the component lead (Fig. 22).

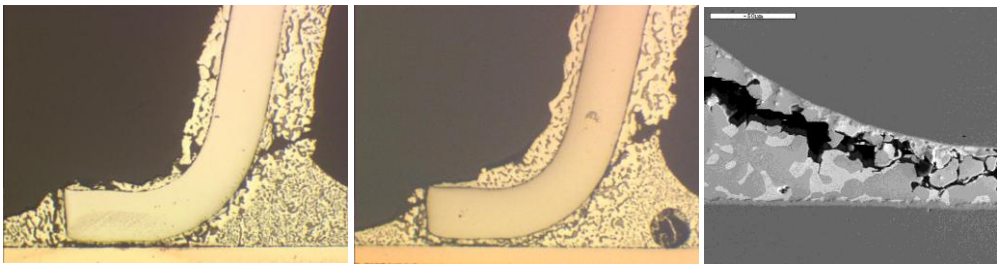

a **b** **c**

Figure 22. **Microstructure of TSOP 54 after thermal cycling, -55°C to 125°C cycling: a – SnPb profile, ImmSn, 1044 cycles, 100x; b – SnPb$^+$ profile, ImmSn, 1155 cycles, 100x; c - SnPb$^+$ profile, ImmSn, 1155 cycles, SEM, 700x.**

Conclusions

The following conclusions are based on the findings of this study:

- Microstructure formation during reflow:
  - Partial or full mixing of Sn-Ag-Cu (SAC) solder balls with Sn-Pb solder occurs during conventional reflow (SnPb profile). After Sn-Pb solder melts, the SAC solder ball begins to dissolve into the molten solder. The degree of dissolution depends on the component type (solder ball size and SAC ball / Sn-Pb solder ratio) and reflow parameters (temperature and time above Sn-Pb solder liquidus (183°C)). The degree of mixing decreases as the ball size increases and the temperature and time decreases.
    - Large components retain significant portions of the initial SAC balls in solder joints reflowed using conventional Sn-Pb profile. The degree of mixing is 30 – 50% and 35 – 45% for PBGA1156 and SBGA 560, respectively.
    - Solder joints in small components such as CSP 132 may be completely mixed independent of its position in the component. Solder joints in other components such as in µBGA 288 may be mixed at the corner and outer layer positions and not mixed in inner rows.

  - If the reflow is done with the temperature above 217°C, the SAC solder balls melt and mix completely with the Sn-Pb solder paste for all types of component. The alloy forming as a result of the SAC ball dissolution or melting together with Sn-Pb solder has a complex composition and a solid – liquid zone (pasty range) of about 30°C.

  - For the SnPb profile conditions, freezing occurs over a wide temperature range starting with the formation of Sn dendrites following by Sn+Pb and/or Sn+Pb+Ag_3Sn ternary eutectic. The Sn phase easily originates from an existing Sn phase in the residual SAC ball or from the clusters in the higher Sn content liquid immediately after its dissolution facilitating the Sn nucleation. The solidification proceeds towards the board side forming a zonal microstructure. The last portion of liquid that contains more eutectic may solidify at the board side and have a Pb-rich zone.

  - The SnPb$^+$ profile eliminates Sn nucleation sites, homogenizes the liquid solder and provides proper conditions for a more uniform solidified microstructure.

  - Detailed examination using SEM, EDX, and DSC did not reveal any evidence of low melting structures in Sn-Bi finished QFP and TSOP solder joints, which is in good agreement with Sn-Pb-Bi system thermodynamics and kinetics of solidification. The Sn-Bi finished QFP solder joint structure is different than the Sn-Pb finished components. They contain primary Sn dendrites in addition to eutectic microstructure.

- ATC Failure Analysis
  - Large ball grid array components PBGA 1156 and SBGA 560 with extended reliability:
    - Completely mixed SAC ball / Sn-Pb solder assembled using the SnPb$^+$ profile have excellent performance at harsh environment cycling and comparable to Sn-Pb fatigue life.
    - Partially mixed joints assembled using SnPb profile may have acceptable reliability unless some microstructure anomalies such as ternary eutectic with high Pb-content and defect accumulation between the intermetallic and the bulk solder form. In this case the main failure mode is not a fatigue fracture at the component side, but interfacial crack propagation between the intermetallic layer and the bulk solder that may be attributed to the insufficient strength of the solder adjacent to the intermetallic layer.

  - Small ball grid array components: µBGA 288 and CSP 132 with limited reliability:

- Completely mixed SAC ball / Sn-Pb solder assembled using the $SnPb^+$ profile have acceptable performance at harsh environment cycling and outperform or comparable to Sn-Pb fatigue life.
- The difference in thermal cycling behavior between the fully and partially mixed SAC ball / Sn-Pb joints are significant. µBGA 288s assembled using the SnPb profile and exhibiting only partial mixing have lower Weibull slopes and therefore earlier failures than the fully mixed joints assembled using the $SnPb^+$ reflow profile. The failure mode of the early failures is the crack propagation between the intermetallic layer and the bulk solder through the area solidified from the last portion of liquid.
- For the CSP 132, there is no statistically significant difference in cycles to failure between $SnPb^+$ and SnPb reflow profiles for the joints formed on ImmSn. For the ENIG boards, the ATC performance of the solder joints after $SnPb^+$ reflow are better. The failure mode of the early failures is the crack propagation between the intermetallic layer and the bulk solder. More work should be done to better understand the mechanism of this type of failure.

- Leaded components QFP 208 and TSOP 54 with Sn-Bi lead finish:
  - The Cu based QFP 208 joints showed excellent performance in harsh environment cycling. No difference in behavior was detected between Sn-Bi and Sn-Pb finished components
  - TSOP 54 with the Alloy 42 lead frame material and Sn-Bi finish had much poorer performance than the QFPs. This was attributed to a higher CTE mismatch due to the Alloy42. The ATC results are similar to those reported in industry for Sn-Pb finished TSOPs. No anomalies in failure mode were detected.

Acknowledgements

The authors would like to thank the following individuals from Celestica and Thales EPM: Russell Brush for ATC testing and data analysis, Zohreh Bagheri for cross-sectioning and metallurgical analyses, Blake Harper for statistical analyses, Marianne Romansky, Thilo Sack, and Jeffrey Kennedy for fruitful technical discussions and manuscript revisions, Julien Perraud and Florent Caperaa for post-assembly analyses, Jean-Guy Chesnay and Wilson Maia for their support in project management and technical guidance.

References

1. F. Hua, R. Aspandiar, C. Anderson, G. Clemons, C. K. Chung and M. Faizul, "Solder Joint Reliability of Sn-Ag-Cu BGA Components Attached with Eutectic Pb-Sn Solder Paste," Surface Mount Technology, 16 (1) (2003), 34-42.
2. P. Snugovsky, A.R. Zebrzezny, M. Kelly and M. Romansky, "Theory and Practice of Lead-free BGA Assembly Using Sn-Pb Solder", CMAP Conference, May 2005.
3. B. Nandagopal, D. Chiang, S. Teng, P. Thune, L. Anderson, R. jay and J. Bath, "Study on Assembly, Rework Process, Microstructures and Mechanical Strength of Backward Compatible Assembly, SMTA, 2005, 861-870.
4. M. Abtew, R. Kinyanjui, N. Nuchsupap, T. Chavasiri, N. Yingyod, P. Saetang, J. Krapun and K. Jikratoke, "Effect of Inert Atmosphere Reflow and Solder Paste Volume on the Microstructure and Mechanical Strength of Mixed Sn-Ag-Cu and Sn-Pb Solder Joints, SMTAI, 2006.
5. M. Cole, M. Kelly, M. Interrante, G. Martin, C. Bergeron, M. Farooq and M. Hoffmeyer, S. Bagheri, P. Snugovsky, Z. Bagheri, M. Romansky, "Reliability Study and Solder Joint Microstructure of Various SnAgCu Ceramic Ball Grid Array (CBGA) Geometries and Alloys," SMTA news,19 (4) (2006), 18-27.
6. H. McCormic, P. Snugovsky, Z. Bagheri, S. Bagheri, C. Hamilton, G. Riccitelli and R. Mohabir, " Mixing Metallurgy: Reliability of SAC Balled Area Array Packages Assembly Using SnPb Solder," SMTA news, 20 (2) (2006), 11-18.
7. D. Hillman, M. Wells, K. Cho, "The Impact of Reflowing A Pb-free Solder Alloy Using a Tin/Lead Solder Alloy Reflow Profile on Solder Joint Integrity," CMAP Conference, Toronto, ON Canada, May 2005.
8. Wickham, M., Zou, L., Dusek, M., Hunt, C., "Measuring the Reliability of Electronics Assemblies During the Transition Period to Lead-Free Soldering", NPL Report DEPC MPR 030, National Physical Laboratory, UK August (2005).
9. T.A. Woodrow, "JCAA/JG-PP Lead-Free Solder Project: -55 to +125 °C Thermal Shock Test; March 1, 2006. Also published in The Proceedings of SMTA International Conference, Rosemont, IL, September 24-28, 2006.
10. O. Maire, C. Munier, S. Bousquet, C. Chastenet, M. Jeremias, "Backward Compatibility of Lead-Free BGA: Microstructural Characterization and Reliability", IPC Soldertec, Malmo, Sweden 2006.
11. D. Hillman, M. Hamand, "Lead-Free (Pb Free) Feasibility Program: Assembly and Testing of a Functional IPC Class 3 Avionics Data Unit", SMTAi 2007, Conference Proceedings, pp. 787 – 797.
12. P Snugovsky, J McMahon, M. Romansky, L. Snugovsky, D. Perovic, J. Rutter "Microstructure and Properties of Sn-Pb Solder Joints with Sn-Bi Finished Components" APEX 2006, Conference Proceedings, pp. 28-01-1 – 28-01-13.

13. P. Snugovsky, J. McMahon, M. Kelly, Z. Bagheri, M. Romansky, “Properties of SMT Solder Joints Formed Between Different Surface and Component Metallization Using Pb-Free and Sn-Pb Pastes”, CMAP 2005, Conference Proceedings.
14. K. Moon, et al, “The Effect of Bi Contamination on the Solidification behavior of Sn-Pb solder”, Journal of Electronic Materials, Vol. 36, No. 6, pp. 676-681, June 2007.
15. D. Hillman, J. Soole, “Solder Joint Integrity Impact of 98%Tin/2%Bismuth Component Surface Finishes”, SMTAi 2007, Conference Proceedings, pp. 597-606.
16. P. Snugovsky, H. McCormick, S. Bagheri, Z. Bagheri, C. Hamilton, M. Romansky, “Microstructure, Defects, and Reliability of Mixed Pb-Free Assemblies”, TMS 2008, Conference Proceedings